



# Thermo-osmosis of a near-critical binary fluid mixture: A general formulation and universal flow direction

Shunsuke Yabunaka <sup>\*</sup>*Advanced Science Research Center, Japan Atomic Energy Agency, Tokai, 319-1195, Japan*Youhei Fujitani <sup>†</sup>*School of Fundamental Science and Technology, Keio University, Yokohama 223-8522, Japan* (Received 20 September 2023; revised 19 March 2024; accepted 14 May 2024; published 18 June 2024)

We consider a binary fluid mixture, which lies in the one-phase region near the demixing critical point, and study its transport through a capillary tube linking two large reservoirs. We assume that short-range interactions cause preferential adsorption of one component onto the tube's wall. The adsorption layer can become much thicker than the molecular size, which enables us to apply hydrodynamics based on a coarse-grained free-energy functional. For transport processes induced by gradients of the pressure, composition, and temperature along a cylindrical tube, we obtain the formulas of the Onsager coefficients to extend our previous results on isothermal transport, assuming the critical composition in the middle of each reservoir in the reference equilibrium state. Among the processes, we focus on thermo-osmosis—mass flow due to a temperature gradient. We explicitly derive a formula for the thermal force density, which is nonvanishing in the adsorption layer and causes thermo-osmosis. This formula for a near-critical binary fluid mixture is an extension of the conventional formula for a one-component fluid, expressed in terms of local excess enthalpy. We predict that the direction of thermo-osmotic flow of a mixture near the upper (lower) consolute point is the same as (opposite to) that of the temperature gradient, irrespective of which component is adsorbed on the wall. Our procedure would also be applied to dynamics of a soft material, whose mesoscopic inhomogeneity can be described by a coarse-grained free-energy functional.

DOI: [10.1103/PhysRevE.109.064610](https://doi.org/10.1103/PhysRevE.109.064610)

## I. INTRODUCTION

Osmotic transport of a fluid through a channel at micrometer, or smaller, scales has gained much attention because it is applied in lab-on-a-chip processes [1–6] and involves fundamental problems in nonequilibrium physics [7–12]. A gradient of temperature (solute concentration) along the channel induces a flow, called thermo-osmosis (diffusio-osmosis), because of force density generated in a heterogeneous layer near the channel wall [13–15]. In particular, the force density in thermo-osmosis, which does not involve the buoyancy responsible for thermal convection, is called the thermal force density. Derjaguin and his coworkers rationalize thermo-osmosis and diffusio-osmosis in terms of the continuum description [16–18]. In addition to these osmotic processes, pressure-driven transport through a micropore or a nanopore has also been actively investigated for applications to separation and purification [19,20].

Studies on thermo-osmosis in liquids date back to Refs. [21,22], where electrolyte solutions were observed to permeate porous membranes. Applying Onsager's reciprocity in the continuum theory, Derjaguin and Sidorenkov (DS) proposed a formula expressing the thermal force density

in terms of the local excess enthalpy for a one-component fluid [13–16]. According to this formula, the direction of the flow is the same as (opposite to) that of the temperature gradient if the excess enthalpy density is negative (positive) everywhere near the wall. This is expected naively by considering that the flow in this direction tends to eliminate the temperature gradient by carrying the fluid with lower (higher) enthalpy to the region with higher (lower) temperature. However, the local excess enthalpy is not easy to access experimentally and is numerically evaluated only on the basis of simplified microscopic models [7,23]. Besides, well-definedness of microscopic expression of excess enthalpy is questioned especially near the surface [7,24]. Therefore, it remains difficult to incorporate detailed microscopic interactions theoretically, and even predicting the flow direction is often challenging [8,23,24]. In Ref. [7], the authors propose an extension of DS's formula for a multicomponent fluid using the continuum description, while questioning its validity in a microscopic slip layer. The validity is numerically examined in Refs. [25,26].

Thermo-osmosis has not been studied in relation to critical phenomena to the best of our knowledge. In the present study, for a binary fluid mixture lying in the one-phase region close to the demixing critical point, we extend our previous study on isothermal dynamics [27] to cover nonisothermal dynamics of thermo-osmosis. Below, this mixture, simply referred to as a mixture, is assumed to be filled in a container composed of

<sup>\*</sup>Contact author: [yabunaka123@gmail.com](mailto:yabunaka123@gmail.com)<sup>†</sup>Contact author: [youhei@appi.keio.ac.jp](mailto:youhei@appi.keio.ac.jp)

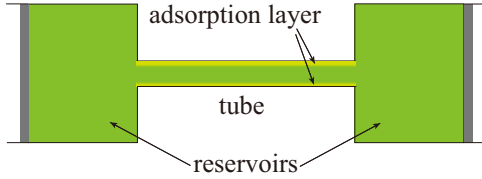


FIG. 1. Schematic of a situation considered in our formulation. A mixture is filled in the container composed of two reservoirs and a capillary tube connecting them. One component drawn in yellow is preferentially adsorbed onto the tube's wall, which is impermeable and adiabatic. There may be preferential adsorption onto the reservoir's wall, which is not assumed in this figure. Thick walls represent pistons. Imposing difference in pressure, composition, and/or temperature between the reservoirs generates mass flow through the tube.

two large reservoirs and a capillary tube connecting them. The tube's wall is impermeable and adiabatic. Differences in temperature, composition, and pressure can be imposed between the two reservoirs (Fig. 1). Between each mixture component and tube's wall, we assume a short-range interaction, which in general attracts one component to the wall more than the other. The resulting preferential adsorption (PA), becoming remarkable owing to large osmotic susceptibility [28,29], has been studied for a long time [30–33]. The adsorption layer can be much thicker than the molecular size when the mixture temperature, denoted by  $T$ , approaches within 1 K of the critical temperature,  $T_c$ , as discussed later. Due to this unique feature of the near-criticality, the continuum description can be justified in studying some processes of the mixture transport [34].

In Ref. [27], applying the hydrodynamics based on a coarse-grained free-energy functional [35], the present authors studied isothermal transport in the linear regime with respect to thermodynamic forces to calculate the involved Onsager coefficients and conductance in diffusio-osmosis. Order-parameter fluctuations in a mixture are significant on length scales smaller than the correlation length, denoted by  $\xi$ , and enhance the transport coefficients to cause universal properties [36–40]. However, the PA prevents the mixture composition in a tube from approaching the critical one, and thus the critical enhancement does not affect diffusio-osmosis of a mixture significantly [27]. Hydrodynamics can be applied to a flow in the tube, where  $\xi$  is locally smaller than a typical length of the flow. It is also suggested in Ref. [27] that, in a critical regime, the mixture velocity due to diffusio-osmosis far from a flat surface should exhibit a power-law dependence on the reduced temperature,  $\tau \equiv (T - T_c)/T_c$ , if the adsorption is sufficiently strong and the composition is critical far from the surface. This originates from the universal order-parameter profile at equilibrium [41,42]. The same power law is numerically suggested for the diffusiphoretic mobility of a colloidal particle in a mixture [43,44]. Universal properties, if confirmed experimentally, would expand our knowledge of the critical phenomena in general.

Our general formulation is described in Secs. II A and II B. We employ the hydrodynamics under inhomogeneous temperature formulated from a coarse-grained free-energy functional [45,46]. The formulation may be extended to

nonisothermal dynamics of various soft materials. Imposing the no-slip condition at the tube's wall and neglecting effects of the tube's edges, we discuss flow fields in the tube in the linear regime in Sec. II C. In Secs. III A and III B, we derive formulas of the Onsager coefficients and a formula of the thermal force density for a cylindrical tube, assuming the total mass density to be homogeneous inside the tube and the mixture composition to be critical in the middle of the reservoir in the reference equilibrium state. The former formulas include extensions of our previous results of Ref. [27] to nonisothermal transport, whereas the latter can be regarded as an extension of DS's formula to a mixture considered here. We apply the renormalized local functional theory [41,47] to specify the free-energy functional in Sec. III C, and rewrite our formulas in Sec. III D. This theory can incorporate the effects of the critical fluctuations in the adsorption layer, where  $\xi$  is inhomogeneous. In Sec. IV we focus on thermo-osmosis to show numerical results and predict that, irrespective of which component is adsorbed on the wall, the flow direction is the same as (opposite to) the direction of the temperature gradient in thermo-osmosis of a mixture near the upper (lower) consolute point. Further discussion and summary are given in Sec. V.

## II. FORMULATION

We write  $\rho_a$  ( $\rho_b$ ) for the mass density of a mixture component named a (b). The sum  $\rho_a + \rho_b$  is denoted by  $\rho$ , which represents the total mass density, whereas the difference  $\rho_a - \rho_b$  is denoted by  $\varphi$ . We write  $c_n$  for the mass fraction  $\rho_n/\rho$  and  $\mu_n$  for the chemical potential conjugate to  $\rho_n$ , where  $n$  is a or b. In an equilibrium mixture with homogeneous mass densities,  $\mu_n$  is a function of  $T$ ,  $c_a$ , and the pressure (denoted by  $P$ ), and is also a function of  $T$ ,  $\rho$ , and  $\varphi$ . We write  $\mu_{\pm}$  for  $(\mu_a \pm \mu_b)/2$ ;  $\rho$  and  $\varphi$  are conjugate to  $\mu_+$  and  $\mu_-$ , respectively. In Fig. 1, difference of a quantity in the left reservoir subtracted from the quantity in the right is indicated by  $\delta$ . For example,  $\delta\mu_a$  denotes the difference in  $\mu_a$  between the reservoirs. If a component is preferentially adsorbed not only onto the tube's wall but also onto the reservoir's wall,  $\rho_n$  is also inhomogeneous in the reservoir. Then  $\delta\rho_n$  indicates the difference in  $\rho_n$  between the central regions of the reservoirs. The difference between the pressures on the pistons is given by  $\delta P$ .

### A. Thermodynamics

The partial volume and partial entropy per unit mass of the component  $n$ , are denoted by  $\bar{v}_n$  and  $\bar{s}_n$ , respectively. In an equilibrium mixture with homogeneous densities, we have

$$\bar{v}_n = \left( \frac{\partial \mu_n}{\partial P} \right)_{T, c_a} \quad \text{and} \quad \bar{s}_n = - \left( \frac{\partial \mu_n}{\partial T} \right)_{P, c_a}, \quad (1)$$

where the subscript of a right parenthesis indicates the fixed variables in the partial differentiation. Writing  $s$  for the entropy per unit volume, we have

$$1 = \bar{v}_a \rho_a + \bar{v}_b \rho_b \quad \text{and} \quad s = \bar{s}_a \rho_a + \bar{s}_b \rho_b \quad (2)$$

at equilibrium with  $\rho_n$  and  $s$  being homogeneous. We write  $\bar{v}_-$  and  $\bar{s}_-$  for  $(\bar{v}_a - \bar{v}_b)/2$  and  $(\bar{s}_a - \bar{s}_b)/2$ , respectively; the

equations in Eq. (1) remain valid after the subscript  $n$  is replaced by  $-$  throughout.

We consider the Helmholtz free-energy functional of a mixture, where fields are coarse grained up to the local correlation length  $\xi$ . A part of the functional is given by the volume integral of a function over the mixture region,  $V_{\text{tot}}$ . The function, denoted by  $f_{\text{bulk}}$ , is assumed to depend on  $\rho_a, \rho_b$ , their gradients, and  $T$ , with the dependence on the gradients being via  $|\nabla\rho_a|^2$ ,  $|\nabla\rho_b|^2$  and  $(\nabla\rho_a) \cdot (\nabla\rho_b)$ . The gradient terms are indispensable because  $\xi$  can be much larger than the length scale where the local equilibrium is defined. The other part, representing the wall-component interaction, is given by the area integral of a function over the interface,  $\partial V_{\text{tot}}$ . This function, denoted by  $f_{\text{surf}}$ , depends on  $\rho_a, \rho_b$ , and  $T$ . Thus, the free-energy functional is given by

$$F[T, \rho_a, \rho_b] = \int_{V_{\text{tot}}} d\mathbf{r} f_{\text{bulk}}(T, \rho_a, \rho_b, \nabla\rho_a, \nabla\rho_b) + \int_{\partial V_{\text{tot}}} dA f_{\text{surf}}(T, \rho_a, \rho_b), \quad (3)$$

where  $T$  and  $\rho_n$  depend on the position  $\mathbf{r}$ . The volume (area) element is represented by  $d\mathbf{r}$  ( $dA$ ). In  $V_{\text{tot}}$ , we write  $u$  for the internal energy per unit volume to have

$$s = -\left(\frac{\partial f_{\text{bulk}}}{\partial T}\right)_{\rho_n, \nabla\rho_n} \quad \text{and} \\ u = f_{\text{bulk}} + Ts = -T^2 \left(\frac{\partial}{\partial T} \frac{f_{\text{bulk}}}{T}\right)_{\rho_n, \nabla\rho_n}. \quad (4)$$

## B. Hydrodynamics

We can neglect order-parameter fluctuations to formulate hydrodynamics on length scales larger than  $\xi$ . The mixture's velocity field,  $\mathbf{v}$ , is defined in the frame fixed to the container. The time derivative of  $\rho$  equals  $-\nabla \cdot (\rho\mathbf{v})$ . In the stationary state, we have

$$0 = \nabla \cdot (\rho\mathbf{v}). \quad (5)$$

Although  $\rho$  is not assumed to be a constant in the dynamics, we have  $\nabla \cdot \mathbf{v} = 0$  for a weak, laminar, and stationary flow in the tube, as mentioned in the next subsection. For this flow, the momentum conservation is represented by

$$2\nabla \cdot (\eta_s \mathbf{E}) = \nabla \cdot \Pi, \quad (6)$$

where  $\mathbf{E}$  is the rate-of-strain tensor,  $\eta_s$  is the shear viscosity dependent on the local composition, and  $\Pi$  is the reversible part of the pressure tensor. As shown later,  $\Pi$  is expressed in terms of  $f_{\text{bulk}}$ . Because of the mass conservation of each component, the time derivative of  $\rho_n$  is equal to the negative of the divergence of its flux, whose deviation from the convective part,  $\rho_n \mathbf{v}$ , gives the diffusion flux, denoted by  $\mathbf{j}_n$ . It is defined so that  $\mathbf{j}_a + \mathbf{j}_b$  vanishes [48]. In the stationary state, we have

$$0 = \nabla \cdot (\varphi\mathbf{v} + \mathbf{j}), \quad (7)$$

where  $\mathbf{j}$  is defined as  $\mathbf{j}_a - \mathbf{j}_b$ . The energy conservation is described in the next subsection.

The scalar pressure  $P$  is given by the negative of the grand-potential density,

$$P = \mu_n \rho_n - f_{\text{bulk}} = \mu_+ \rho + \mu_- \varphi - f_{\text{bulk}}. \quad (8)$$

If  $T$  is homogeneous,  $\mu_n(\mathbf{r})$  is given by the functional derivative of the first term on the right-hand side (r.h.s.) of Eq. (3) with respect to  $\rho_n(\mathbf{r})$  in  $V_{\text{tot}}$ . Otherwise, it is given by

$$\mu_n = \frac{\partial f_{\text{bulk}}}{\partial \rho_n} - T \nabla \cdot \left[ \frac{1}{T} \frac{\partial f_{\text{bulk}}}{\partial (\nabla \rho_n)} \right]. \quad (9)$$

With  $\mathbf{1}$  denoting the identity tensor of order two and repeated indices summed up, we have

$$\Pi = P\mathbf{1} + (\nabla \rho_n) \frac{\partial f_{\text{bulk}}}{\partial (\nabla \rho_n)}, \quad (10)$$

which is symmetric. The gradient terms in  $f_{\text{bulk}}$  can make  $\mu_n$  and  $\Pi$  dependent on the gradient terms and make  $\Pi$  nonisotropic. Equations (9) and (10) are derived for a one-component fluid in Ref. [45] and are applied in a straightforward way to a binary fluid mixture in Ref. [46]. The previous derivation is not applicable to  $f_{\text{bulk}}$  specified in Sec. III C. The coefficient of the square-gradient term,  $M_-/2$  in Eq. (37), depends on  $T$  slightly nonlinearly although the linear dependence was assumed in the previous derivation. In Appendix A we show a more general derivation, which can be applied to  $f_{\text{bulk}}$  of Eq. (37). Notably, this derivation remains relevant to our later calculation of thermo-osmosis under the linear regime, because the hydrodynamic equations including this nonlinearity must be derived before their linearization with respect to the temperature gradient. Equations (9) and (10) yield an extended Gibbs-Duhem relation

$$\nabla \cdot \Pi = \rho_n \nabla \mu_n + s \nabla T + \frac{\nabla T}{T} \cdot \frac{\partial f_{\text{bulk}}}{\partial (\nabla \rho_n)} \nabla \rho_n, \quad (11)$$

which is consistent with principles of linear nonequilibrium thermodynamics; Eq. (11) guarantees positive entropy production rate after combined with irreversible terms and the Onsager's reciprocity for osmotic fluxes through the tube. The former is shown in Ref. [45], whereas the latter is mentioned below Eq. (24) in the next subsection.

We write  $\mathcal{M}_{nR}$  and  $\mathcal{U}_R$  for the total mass of the component  $n$  and the mixture's internal energy in the right reservoir of Fig. 1, respectively. We have a flow in the tube by imposing the thermodynamic forces,  $-\delta(P/T)$ ,  $-\delta(\mu_-/T)$ , and  $\delta(1/T)$ , on an equilibrium mixture. This equilibrium state, referred to as reference state, is assumed to be close to the critical point. In this section, we do not specify the reference state further for a general formulation. A superscript (ref) is added to a quantity in the middle of a reservoir in the reference state. As shown in Appendix B, the thermodynamic fluxes conjugate to the thermodynamic forces, denoted by  $\mathcal{I}$ ,  $\mathcal{J}$ , and  $\mathcal{K}$ , are given by

$$\begin{bmatrix} \mathcal{I} \\ \mathcal{J} \\ \mathcal{K} \end{bmatrix} = \begin{bmatrix} 1/\rho^{(\text{ref})} & 1/\rho^{(\text{ref})} & 0 \\ 2c_b^{(\text{ref})} & -2c_a^{(\text{ref})} & 0 \\ -u^{(\text{ref})}/\rho^{(\text{ref})} & -u^{(\text{ref})}/\rho^{(\text{ref})} & 1 \end{bmatrix} \begin{bmatrix} d\mathcal{M}_{aR}/(dt) \\ d\mathcal{M}_{bR}/(dt) \\ d\mathcal{U}_R/(dt) \end{bmatrix}, \quad (12)$$

where  $t$  denotes the time. We can define a  $3 \times 3$  matrix  $L$ , composed of the Onsager coefficients, so that the linear phenomenological equation

$$[\mathcal{I}, \mathcal{J}, \mathcal{K}]^T = L[-\delta(P/T), -\delta(\mu_-/T), \delta(1/T)]^T \quad (13)$$

holds, with the superscript T indicating the transpose. We use Eq. (1) to obtain

$$\delta\mu_- = -\bar{s}_-^{(\text{ref})}\delta T + \bar{v}_-^{(\text{ref})}\delta P + \left(\frac{\partial\mu_-}{\partial c_a}\right)_{T,P} \delta c_a, \quad (14)$$

where the partial derivative is evaluated in the middle of the reservoir in the reference state. Thus, the thermodynamic forces in Eq. (13) are determined by  $\delta T$ ,  $\delta P$ , and  $\delta c_a$ , and determine  $\delta\mu_+$  because the usual Gibbs-Duhem (GD) relation gives

$$\delta P = \rho_n^{(\text{ref})}\delta\mu_n + s^{(\text{ref})}\delta T = \rho^{(\text{ref})}\delta\mu_+ + \varphi^{(\text{ref})}\delta\mu_- + s^{(\text{ref})}\delta T. \quad (15)$$

### C. Fields in the tube

We assume that  $\delta T$ ,  $\delta P$ , and  $\delta c_a$  are proportional to a dimensionless smallness parameter  $\varepsilon$  and expand the fields with respect to  $\varepsilon$ . The superscripts (0) and (1) are used to indicate the order of  $\varepsilon$ . We have  $\mu_{\pm} = \mu_{\pm}^{(0)} + \varepsilon\mu_{\pm}^{(1)}$  up to the order of  $\varepsilon$ ,  $\mu_{\pm}^{(0)} = \mu_{\pm}^{(\text{ref})}$ , and  $T^{(0)} = T^{(\text{ref})}$ . In contrast,  $\rho_n^{(0)}$  becomes inhomogeneous and different from  $\rho_n^{(\text{ref})}$  in the presence of PA. Because the fields are assumed to be coarse grained up to  $\xi$ , the mass densities at the equilibrium specified by  $T^{(\text{ref})}$  and  $\mu_n^{(\text{ref})}$  minimize the grand-potential functional,

$$F[T^{(\text{ref})}, \rho_a, \rho_b] - \int_{V_{\text{tot}}} d\mathbf{r} [\mu_+^{(\text{ref})}\rho(\mathbf{r}) + \mu_-^{(\text{ref})}\varphi(\mathbf{r})]. \quad (16)$$

Thus,  $\rho_n^{(0)}$  is the solution of Eq. (9) with  $T$  and  $\mu_n$  replaced by  $T^{(\text{ref})}$  and  $\mu_n^{(\text{ref})}$ , respectively, together with the boundary conditions given by Eq. (A8). Below we consider stationary and laminar flow in the tube at the order of  $\varepsilon$ . The mixture is assumed to remain in one-phase region throughout inside the container. As in the previous study [27], we assume that the tube is so long and thin that effects of the tube's edges on the flow are negligible. We regard  $\delta\mu_n$  and  $\delta T$  as equal to the differences in  $\mu_n$  and  $T$  between the edges, respectively;  $\mu_n$  and  $T$  are regarded as homogeneous over the tube's cross section at each edge.

Assuming the tube to extend along the  $z$  axis with the same cross section, we take the Cartesian coordinates  $(x, y, z)$  so that the right reservoir lies on the positive  $z$  side. A field with the superscript (0), such as  $\rho_n^{(0)}$ , is independent of  $z$  in the tube. Thus, for the laminar flow with  $v_x = v_y = 0$ , Eq. (5) gives

$$0 = \nabla \cdot \mathbf{v}^{(1)} = \partial_z v_z^{(1)}, \quad (17)$$

where  $\partial_z$  denotes the partial derivative with respect to  $z$ . This justifies Eq. (6) in the tube up to the order of  $\varepsilon$ . We write  $\eta_s^{(0)}$  for  $\eta_s$  evaluated at  $\varepsilon = 0$ ;  $\eta_s^{(0)}$  depends on  $\varphi^{(0)}$ . In the absence of PA,  $\rho_n^{(0)}$  and  $\eta_s^{(0)}$  are homogeneous, and thus Eq. (6) gives  $\eta_s^{(0)}\Delta\mathbf{v}^{(1)} = \nabla P^{(1)}$ .

We write  $e$  for the total-energy density, given by  $u + \rho|\mathbf{v}|^2/2$ , to have  $u^{(0)} = e^{(0)}$ . The heat flux, denoted by  $\mathbf{j}_q$ , is defined so that the Eulerian time derivative of  $e$  equals  $-\nabla \cdot (e\mathbf{v} + \mathbf{v} \cdot \Pi + \mathbf{j}_q)$ . In a stationary state in the tube, the energy conservation gives

$$0 = \nabla \cdot (u^{(0)}\mathbf{v}^{(1)} + \mathbf{v}^{(1)} \cdot \Pi^{(0)} + \mathbf{j}_q^{(1)}). \quad (18)$$

The transport coefficients,  $\Lambda$ ,  $\lambda$ , and  $\kappa$  are defined so that we have [48,49]

$$\mathbf{j} = -T\Lambda\nabla\frac{\mu_-}{T} + \kappa\nabla\frac{1}{T} \quad \text{and} \quad \mathbf{j}_q = -\kappa\nabla\frac{\mu_-}{T} + \lambda\nabla\frac{1}{T}. \quad (19)$$

The coefficients depend on  $\xi$  owing to the critical enhancement. If evaluated using  $\xi$  at  $\varepsilon = 0$ , they are denoted by  $\Lambda^{(0)}$ ,  $\kappa^{(0)}$ , and  $\lambda^{(0)}$ , respectively, and are independent of  $z$ . In Eq. (19) at the order of  $\varepsilon$ , we can use  $T^{(0)}\Lambda^{(0)}$ ,  $\kappa^{(0)}$ , and  $\lambda^{(0)}$  for  $T\Lambda$ ,  $\kappa$ , and  $\lambda$ , respectively.

As calculated in Appendix C, the  $z$  component of Eq. (6) at the order of  $\varepsilon$  is found to become

$$\begin{aligned} \varepsilon\bar{\nabla} \cdot (\eta_s^{(0)}\bar{\nabla}v_z^{(1)}) \\ = \frac{T^{(0)}}{L_{\text{tube}}} \left\{ \frac{\rho^{(0)}}{\rho^{(\text{ref})}}\delta\left(\frac{P}{T}\right) + \left(\varphi^{(0)} - \frac{\rho^{(0)}\varphi^{(\text{ref})}}{\rho^{(\text{ref})}}\right)\delta\left(\frac{\mu_-}{T}\right) \right. \\ \left. + \left(\frac{\rho^{(0)}u^{(\text{ref})}}{\rho^{(\text{ref})}} - u^{(0)} - P^{(0)}\right)\delta\left(\frac{1}{T}\right) \right\} \end{aligned} \quad (20)$$

in the tube, whose length is denoted by  $L_{\text{tube}}$ . Here,  $\bar{\nabla}$  represents the two-dimensional nabla on the  $(x, y)$  plane with  $v_z^{(1)}$  regarded as a scalar. Equation (20) determines  $v_z^{(1)}$  together with the no-slip boundary condition at the wall;  $v_z^{(1)}$  is independent of  $z$  because of Eq. (17). As shown in Appendix C, the  $x$  and  $y$  components of  $\mathbf{j}^{(1)}$  and  $\mathbf{j}_q^{(1)}$  vanish in the tube, and Eq. (19) yields

$$\varepsilon j_z^{(1)} = \frac{1}{L_{\text{tube}}} \left[ T^{(0)}\Lambda^{(0)}\delta\left(\frac{-\mu_-}{T}\right) + \kappa^{(0)}\delta\left(\frac{1}{T}\right) \right] \quad (21)$$

and

$$\varepsilon j_{qz}^{(1)} = \frac{1}{L_{\text{tube}}} \left[ \kappa^{(0)}\delta\left(\frac{-\mu_-}{T}\right) + \lambda^{(0)}\delta\left(\frac{1}{T}\right) \right] \quad (22)$$

in the tube. Up to the order of  $\varepsilon$ ,  $d\mathcal{M}_{\text{NR}}/(dt)$  and  $d\mathcal{U}_{\text{R}}/(dt)$  are respectively given by the area integral of  $\varepsilon(\rho_n^{(0)}v_z^{(1)} + j_{nz}^{(1)})$  and that of  $\varepsilon(u^{(0)} + P^{(0)})v_z^{(1)} + \varepsilon j_{qz}^{(1)}$  over a tube's cross section, which is denoted by  $S_{\text{tube}}$ . Thus, we use Eq. (12) to obtain

$$\begin{aligned} \mathcal{I} &= \frac{\varepsilon}{\rho^{(\text{ref})}} \int_{S_{\text{tube}}} dA \rho^{(0)}v_z^{(1)}, \\ \mathcal{J} &= \varepsilon \int_{S_{\text{tube}}} dA \left[ \left(\varphi^{(0)} - \frac{\rho^{(0)}\varphi^{(\text{ref})}}{\rho^{(\text{ref})}}\right)v_z^{(1)} + j_z^{(1)} \right] \end{aligned} \quad (23)$$

and

$$\mathcal{K} = \varepsilon \int_{S_{\text{tube}}} dA \left[ \left(u^{(0)} + P^{(0)} - \frac{\rho^{(0)}u^{(\text{ref})}}{\rho^{(\text{ref})}}\right)v_z^{(1)} + j_{qz}^{(1)} \right]. \quad (24)$$

In Appendix B, our formulation up to here is shown to be consistent with Onsager's reciprocal relation, as it should be. Because of Eq. (8),  $P^{(0)}$  can be inhomogeneous on a tube's cross section in the presence of PA. In its absence, because  $P^{(0)}$  is homogeneously equal to  $P^{(\text{ref})}$ , the r.h.s. of Eq. (20), and thus  $v_z^{(1)}$ , vanish when  $\delta P$  vanishes. This is consistent with the results in Chapter XV-5 of Ref. [48].

With the subscript c, we refer to the value at the critical point under the pressure  $P^{(\text{ref})}$ . The deviation of  $\varphi$  from its value at the critical point,  $\varphi - \varphi_c$ , plays a role of the order parameter of phase separation and is denoted by  $\psi$ . In



the fluctuations about the equilibrium, correlated clusters of  $\psi$  are randomly convected on length scales smaller than  $\xi$ . On larger length scales, the convection is averaged out to enhance the transport coefficient for the interdiffusion in a mixture at the critical composition, as mentioned in Sec. I. The critical enhancement suppresses the critical slowing down of the relaxation of the two-time correlation function of  $\psi$ . This function follows the diffusion equation. According to the mode-coupling theory [36], the singular part of the diffusion coefficient coincides with the self-diffusion coefficient of a rigid sphere with the radius being equal to  $\xi$ . This result is slightly modified by the dynamic renormalization-group calculation for the model H, with the weak singularity of  $\eta_s$  taken into account [37,38,40,50,51]. We write  $z_\psi$  for the dynamic critical exponent for the order-parameter fluctuations and use  $z_\psi = 3.067$  [52,53]. The singular part of  $\eta_s$ , denoted by  $\eta_{\text{sing}}$ , becomes proportional to  $\xi^{z_\psi-3}$  as the critical point is approached; details are mentioned in Appendix E of Ref. [27]. Because multiplying the diffusion coefficient by the osmotic susceptibility, denoted by  $\chi$ , gives the transport coefficient  $\Lambda$ , we have

$$\Lambda = \frac{\chi R k_B T_c}{\xi \eta_{\text{sing}}}, \quad (25)$$

where  $R$  is a universal constant close to  $1/(6\pi)$  and  $k_B$  is the Boltzmann constant. The regular part of  $\Lambda$  is usually negligible in the critical regime, judging from the data in Ref. [54], for example. The partial enthalpy per unit mass of the component  $n$ , denoted by  $\bar{H}_n$ , is given by

$$\bar{H}_n = \mu_n + T \bar{s}_n = -T^2 \left( \frac{\partial \mu_n}{\partial T} \right)_{P,c_a}. \quad (26)$$

We neglect the regular parts in the results of Ref. [55], as shown in Appendix D, and use

$$\kappa = \Lambda T \bar{H}_- \quad \text{and} \quad \lambda = \Lambda T (\bar{H}_-)^2, \quad (27)$$

where  $\bar{H}_-$  is defined as  $(\bar{H}_a - \bar{H}_b)/2$ .

Equation (25) holds at equilibrium with the critical composition. In our problem, to evaluate  $\Lambda^{(0)}$ , we simply extend this result to a homogeneous off-critical composition and use the extended result even when the composition is inhomogeneous. Hence, we evaluate the r.h.s. of Eq. (25) by using  $T^{(0)}$ ,  $\psi^{(0)}(\mathbf{r})$ , and the resulting local value of  $\xi$ , to obtain  $\Lambda^{(0)}$ . This is the same procedure as used in Refs. [27,35]. Likewise, we obtain  $\kappa^{(0)}$  and  $\lambda^{(0)}$  in the dynamics by replacing  $\Lambda$ ,  $T$ , and  $\bar{H}_-$  with  $\Lambda^{(0)}$ ,  $T^{(0)}$ , and  $\bar{H}_-^{(0)}$ , respectively, in Eq. (27). Like  $\Lambda^{(0)}$ ,  $\bar{H}_-^{(0)}$  is evaluated using the local composition at  $\varepsilon = 0$ .

### III. CALCULATION UNDER SOME SPECIFICATIONS

We specify the problem by making the following assumptions. First, we assume  $f_{\text{surf}}$  to be independent of  $\rho$ , which means  $\rho^{(0)} = \rho^{(\text{ref})}$ . Second, we assume the critical composition in the middle of the reservoir in the reference state, i.e.,  $\psi^{(\text{ref})} = 0$ . Third, we assume the tube to be a cylinder with the radius of  $r_{\text{tube}}$ . In the tube, a field depends only on the distance from the central axis,  $r$ , on a cross section, and we can write  $\psi^{(0)}(r)$ ,  $\eta_s^{(0)}(r)$ ,  $v_z^{(1)}(r)$ , and  $j_z^{(1)}(r)$ , for example. The left-hand side (l.h.s.) of Eq. (20) becomes  $\varepsilon r^{-1} \partial_r (r \eta_s^{(0)} \partial_r v_z^{(1)})$ ;  $v_z^{(1)}$  vanishes at  $r = r_{\text{tube}}$  owing to the no-slip condition, and  $\partial_r v_z^{(1)}$

vanishes at  $r = 0$  owing to the axisymmetry and smoothness of  $v_z^{(1)}$ . Thus, we obtain  $v_z^{(1)}$  in the tube, as shown by Eq. (C8). Substituting this result, together with Eqs. (21) and (22), into Eqs. (23) and (24) yields formulas for the Onsager coefficients  $L_{ij}$ , as described in Sec. III A.

#### A. Formulas for the Onsager coefficients

A dimensionless radial distance  $\hat{r}$  is defined as  $r/r_{\text{tube}}$ . We define  $T_*$  so that  $\xi$  becomes  $r_{\text{tube}}$  for  $\psi = 0$  at  $T = T_*$ . A characteristic order parameter  $\psi_*$  is defined so that  $\xi$  becomes  $r_{\text{tube}}$  for  $\psi = \psi_*$  at  $T = T_c$ . A dimensionless order parameter at  $\varepsilon = 0$ ,  $\hat{\psi}^{(0)}(\hat{r})$ , is defined as  $\psi^{(0)}(\hat{r} r_{\text{tube}})/\psi_*$ . A characteristic chemical potential,  $\mu_*$ , is defined as

$$\mu_* = \frac{k_B T_*}{3u^* r_{\text{tube}}^3 \psi_*}, \quad (28)$$

where  $u^*$  is the scaled coupling constant at the Wilson-Fisher fixed point and equals  $2\pi^2/9$  at the one loop order. This value is used in the renormalized local functional theory [47] and  $\mu_*$  is defined as above for convenience after Sec. III C. We define  $\eta_*$  and  $\Lambda_*$  as  $\eta_{\text{sing}}$  and  $\Lambda$  at  $\psi = 0$  and  $T = T_*$ , respectively. Dimensionless transport coefficients  $\hat{\eta}(\hat{r})$  and  $\hat{\Lambda}(\hat{r})$  are defined as  $\eta_s^{(0)}/\eta_*$  and  $T^{(0)}\Lambda^{(0)}/(T_*\Lambda_*)$  evaluated at  $r = \hat{r} r_{\text{tube}}$ , respectively. The flow rate of Hagen-Poiseuille flow of a fluid, with the viscosity being  $\eta_*$ , driven by the pressure gradient  $\mu_* \psi_*/L_{\text{tube}}$ , is denoted by  $\mathcal{I}_*$  and is given by

$$\mathcal{I}_* = \frac{\pi r_{\text{tube}}^4 \mu_* \psi_*}{8\eta_* L_{\text{tube}}}. \quad (29)$$

We define a functional  $\Omega[g_1, g_2]$ , where  $g_1$  and  $g_2$  are functions, as

$$\begin{aligned} \Omega[g_1, g_2] &= 16 \int_0^1 dq_1 q_1 g_1(q_1) \int_{q_1}^1 dq_2 \frac{1}{q_2 \hat{\eta}(q_2)} \\ &\times \int_0^{q_2} dq_3 q_3 g_2(q_3), \end{aligned} \quad (30)$$

which is found to be equal to  $\Omega[g_2, g_1]$  by exchanging the order of integrals. The formulas for  $L_{11}$ ,  $L_{12}$ , and  $L_{22}$ , given by Eqs. (C9) and (C10), are essentially the same as obtained in Ref. [27]. Introducing

$$\hat{Y}^{(0)}(\hat{r}) = \frac{1}{\mu_* \psi_*} [u^{(0)} - u^{(\text{ref})} + P^{(0)}] \quad \text{and} \quad \hat{H}_-^{(0)}(\hat{r}) = \frac{\bar{H}_-^{(0)}}{\mu_*}, \quad (31)$$

where  $u^{(0)}$ ,  $P^{(0)}$ , and  $\bar{H}_-^{(0)}$  are evaluated at  $r = \hat{r} r_{\text{tube}}$ , we obtain new formulas:

$$L_{13} = L_{31} = \mathcal{I}_* T^{(0)} \Omega[1, \hat{Y}^{(0)}], \quad (32)$$

$$\begin{aligned} L_{23} = L_{32} &= \mathcal{I}_* \psi_* T^{(0)} \Omega[\hat{\psi}^{(0)}, \hat{Y}^{(0)}] \\ &+ 2\pi r_{\text{tube}}^2 \frac{\mu_* \Lambda_* T_*}{L_{\text{tube}}} \int_0^1 d\hat{r} \hat{r} \hat{\Lambda}(\hat{r}) \hat{H}_-^{(0)}(\hat{r}), \end{aligned} \quad (33)$$

and

$$\begin{aligned} L_{33} &= \mathcal{I}_* \mu_* \psi_* T^{(0)} \Omega[\hat{Y}^{(0)}, \hat{Y}^{(0)}] \\ &+ 2\pi r_{\text{tube}}^2 \frac{\mu_*^2 \Lambda_* T_*}{L_{\text{tube}}} \int_0^1 d\hat{r} \hat{r} \hat{\Lambda}(\hat{r}) [\hat{H}_-^{(0)}(\hat{r})]^2. \end{aligned} \quad (34)$$

We use Eq. (27) to derive the last terms of these two equations.

### B. Formulas for thermo-osmosis

The thermal force density causes thermo-osmosis. This density on a tube's cross section in the linear regime, denoted by  $\sigma_z^{(\text{th})}$ , is given by the negative of the r.h.s. of Eq. (20), or the  $z$  component of  $-\varepsilon \nabla \cdot \Pi^{(1)}$ , under  $\delta T \neq 0$  and  $\delta P = \delta c_a = 0$ . We have

$$\sigma_z^{(\text{th})}(r) = -\frac{\delta T}{T^{(0)}L_{\text{tube}}}(u^{(0)}(r) + P^{(0)}(r) - u^{(\text{ref})} - P^{(\text{ref})} - \bar{H}_-^{(\text{ref})}\psi^{(0)}). \quad (35)$$

The factor  $\bar{H}_-^{(\text{ref})}$  above is derived by rewriting  $\delta(\mu_-/T)$  in Eq. (20) with the aid of Eqs. (14) and (26). The first four terms in the parentheses above can be interpreted as the excess enthalpy density in DS's formula for a one-component fluid; the enthalpy density  $u + P$  is calculated using Eqs. (4) and (8). In the presence of PA,  $\Pi_{zz}^{(0)} = P^{(0)}$  is equal to neither  $\Pi_{xx}^{(0)}$  nor  $\Pi_{yy}^{(0)}$ . Thus, Eq. (35) is consistent with the claim that the  $zz$  component should be involved in the thermal force density [7,15].

Here, we compare our derivation of the thermal force density with the corresponding part in Ref. [7], which is mentioned in Sec. I. Because the sum of the last three terms in the parentheses of Eq. (35) equals  $-\rho_a^{(0)}\bar{H}_a^{(\text{ref})} - \rho_b^{(0)}\bar{H}_b^{(\text{ref})}$ , the negative of Eq. (35) formally coincides with the r.h.s. of Eq. (5) of Ref. [7], where the r.h.s. is treated as the negative of the thermal force density. However, its l.h.s.,  $\partial_z \Pi_{zz}$  in our notation, is not equal to  $-\sigma_z^{(\text{th})}$  in general, since  $\partial_x \Pi_{xz} + \partial_y \Pi_{yz}$  does not vanish in the presence of PA;  $\Pi$  can have off-diagonal components in our problem. In Ref. [7], this sum  $\partial_x \Pi_{xz} + \partial_y \Pi_{yz}$  is also missing in the l.h.s. of Eq. (2), which the authors employ as an extended GD relation in deriving their Eq. (5). In the present study, we use our Eq. (11), whose l.h.s. includes  $\partial_x \Pi_{xz} + \partial_y \Pi_{yz}$ , as an extended GD relation to derive Eq. (35), consistently with principles of linear nonequilibrium thermodynamics.

The superscript (th) is used to indicate a result in the linear regime for thermo-osmosis, where the  $z$  component of the velocity is found from Eq. (20) to be given by

$$v_z^{(\text{th})}(r) = \int_r^{r_{\text{tube}}} dr_1 \frac{1}{r_1 \eta_s^{(0)}(r_1)} \int_0^{r_1} dr_2 r_2 \sigma_z^{(\text{th})}(r_2). \quad (36)$$

Integrating  $\rho^{(\text{ref})}v_z^{(\text{th})}(r)$  over the tube's cross-section gives the total mass flow rate, for which we write  $d\mathcal{M}_R^{(\text{th})}/(dt)$ . Using the free-energy functional introduced in Sec. III C, we rewrite Eq. (35) and give an explicit expression of  $d\mathcal{M}_R^{(\text{th})}/(dt)$  in Sec. III D. In the absence of PA, because Eq. (35) vanishes,  $v_z^{(\text{th})}$  and  $d\mathcal{M}_R^{(\text{th})}/(dt)$  vanish. Thus, in our formulation, thermo-osmosis of a mixture occurs only in the presence of PA. The expression of  $d\mathcal{M}_R^{(\text{th})}/(dt)$  is also derived via the formulas for  $L_{ij}$ , as mentioned in Appendix C.

### C. Free-energy functional in the renormalized local functional theory

The scaled reduced temperature  $\hat{\tau}$  is defined as  $\tau/\tau_*$ , where  $\tau_*$  is defined as  $|T_* - T_c|/T_c$ . In the one-phase region, we have

$\tau > 0$  near the upper consolute (UC) point and  $\tau < 0$  near the lower consolute (LC) point [56–58]. Using the conventional notation, we write  $\alpha, \beta, \gamma, \nu$ , and  $\eta$  for the critical exponents of a mixture. We adopt  $\nu = 0.630$  and  $\eta = 0.0364$  [59]; the (hyper)scaling relations give  $2\beta + \gamma = 3\nu = 2 - \alpha$  and  $\gamma = \nu(2 - \eta)$ . In the reference state, the mixture has  $\psi = 0$  in the absence of PA. In this situation, with  $\xi_0$  denoting a material constant,  $\xi$  is given by  $\xi_0|\tau|^{-\nu}$ , for which we write  $\xi^{(\text{ref})}$ .

The reference state in the absence of PA is obtained by changing  $T$  from the critical point with  $P = P^{(\text{ref})} = P_c$  and  $\psi = 0$  being fixed. The chemical potentials,  $\mu_a^{(\text{ref})}$  and  $\mu_b^{(\text{ref})}$ , are tuned so that this change is realized. Thus, the  $\varphi$ -dependent part for the bulk of a mixture in Eq. (16) can be obtained by coarse graining the bare  $\psi^4$  model up to  $\xi$  under no external field [47]. The bare model is defined at a microscopic scale and identifies the order-parameter fluctuations with spacial resolution much smaller than  $\xi$ . We can regard the coarse-grained average profile as maximizing the probability density functional coarse grained up to  $\xi$ , by assuming the fluctuations to be negligible after coarse graining [47]. This is consistent with the statement given at Eq. (16). We assume

$$f_{\text{bulk}} = -\frac{CT\tau^2}{2} + u_c - s_c T + f_-(\psi) + \frac{M_-}{2}|\nabla\psi|^2 + f_+(\rho). \quad (37)$$

Although the variable  $\tau$  is dropped for conciseness,  $f_+$  is a regular function of  $\rho$  and  $\tau$ , and  $f_-$  is a function of  $\psi$  and  $\tau$ . The coefficient  $M_-$  is described later;  $u_c$  and  $s_c$  respectively represent the values of  $u$  and  $s$  at the critical point. The coefficient  $C$  involves the fluctuations of the internal-energy density. In the critical regime, the singular contribution to  $C$  [39,60] becomes equal to  $2k_B\xi_0^{-3}|\tau|^{-\alpha}$  multiplied by a universal number, as mentioned in footnote 51 of Ref. [47]. We neglect coupling between  $\rho$  and  $\varphi$  in Eq. (37) because  $\rho$  can be regarded as a constant approximately. Some details on these points are mentioned in Appendix E. As shown in Eq. (E1), we can define  $A_0$  so that the bare  $\psi^4$  model has a term  $A_0\tau\psi^2/2$ , which is positive in the one-phase region. Thus,  $A_0$  is positive (negative) near a UC (LC) point [39]. The sign is maintained in the coarse-graining procedure. We use the coarse-grained result given by the renormalized local functional theory (RLFT) [47].

In the RLFT,  $\omega$  is defined as  $(\xi_0/\xi)^{1/\nu}$  and  $M_-$  is given by  $k_B T C_1 \omega^{-\eta\nu}$  with  $C_1 (> 0)$  being a material constant. The self-consistent condition,  $\omega = |\tau| + C_2 \omega^{1-2\beta} \psi^2$ , determines how  $\xi$  depends on  $\tau$  and  $\psi$ , where the constant  $C_2$  equals  $3u^*C_1\xi_0$ . This condition gives

$$\tau_* = \left(\frac{\xi_0}{r_{\text{tube}}}\right)^{1/\nu} \quad \text{and} \quad \psi_* = \frac{\tau_*^\beta}{\sqrt{C_2}}. \quad (38)$$

Defining a dimensionless function  $\hat{f}$  as

$$\hat{f}(\hat{\psi}) = \frac{1}{2}\hat{\omega}^{\nu-1}|\hat{\tau}|\hat{\psi}^2 + \frac{1}{12}\hat{\omega}^{\nu-2\beta}\hat{\psi}^4, \quad (39)$$

where  $\hat{\psi} \equiv \psi/\psi_*$ ,  $\hat{\tau} \equiv \tau/\tau_*$ , and  $\hat{\omega} \equiv \omega/\tau_*$  are used, we have

$$f_-(\psi) + \frac{M_-}{2}|\nabla\psi|^2 = \mu_-^{(\text{ref})}\varphi + \frac{\mu_*\psi_*T}{T_*}\hat{f}(\hat{\psi}) + \frac{\mu_*\psi_*T}{2T_*}\hat{\omega}^{-\eta\nu}|r_{\text{tube}}\nabla\hat{\psi}|^2. \quad (40)$$

As already explained,  $\mu_-^{(\text{ref})}$  is determined so that the reference state at  $T$  is realized;  $\mu_-^{(\text{ref})}$  depends on  $T$ . The sum of the second and third terms on the r.h.s. above is  $k_B T$  multiplied by the coarse-grained result of the  $\psi^4$  model under no external field. The self-consistent condition is rewritten as

$$\hat{\omega} = |\hat{\tau}| + \hat{\omega}^{1-2\beta} \hat{\psi}^2, \quad (41)$$

which means that  $\hat{\omega}$  is a function of  $\hat{\psi}$  and  $\hat{\tau}$ . It is even with respect to  $\hat{\psi}$ , and hence  $\hat{f}(\hat{\psi})$  is an even function. The function  $\hat{f}(\hat{\psi})$  also depends on  $\hat{\tau}$ , but the variable  $\hat{\tau}$  is dropped for conciseness. The osmotic susceptibility  $\chi$  is given by the inverse of the second partial derivative of  $f_-$  with respect to  $\psi$ ,  $1/f''(\psi)$ , where the prime indicates the differentiation with respect to the variable shown explicitly. The partial derivative  $\partial \hat{f}/(\partial \hat{\tau})$ , appearing in the later calculation, equals

$$\frac{\pm 1}{2} \hat{\omega}^{\gamma-1} \hat{\psi}^2 + \frac{\partial \hat{\omega}}{\partial \hat{\tau}} \left( \frac{\gamma-1}{2} \hat{\omega}^{\gamma-2} |\hat{\tau}| \hat{\psi}^2 + \frac{\gamma-2\beta}{12} \hat{\omega}^{\gamma-2\beta-1} \hat{\psi}^4 \right), \quad (42)$$

where Eq. (41) gives

$$\frac{\partial \hat{\omega}}{\partial \hat{\tau}} = \frac{\pm 1}{1 + (2\beta-1) \hat{\omega}^{-2\beta} \hat{\psi}^2}. \quad (43)$$

The same sign as  $\tau$  is taken in each double sign of these equations. The first term on the r.h.s. of Eq. (39) originates from  $A_0 \tau \psi^2/2$  in the bare model, and the first term of Eq. (42) from  $A_0 \psi^2/2$ . Equation (41) gives  $|\hat{\psi}|^{1/\beta} < \hat{\omega}$  and  $|\hat{\tau}| < \hat{\omega}$ . For  $\hat{\psi} \neq 0$ , the sign of Eq. (42), or that of  $\partial \hat{f}/(\partial \hat{\tau})$ , coincides with that of  $\tau$ , considering  $\beta = 0.326$  and  $\gamma = 1.24$ . If  $|\hat{\tau}|$  is much smaller than  $\hat{\omega}$ , Eq. (41) gives  $|\hat{\psi}|^{1/\beta} \approx \hat{\omega}$ , and thus Eq. (43) is approximately equal to  $\pm 1/(2\beta)$ . Then, in Eq. (42), the first term is found to be dominant over the rest. If  $|\hat{\tau}|$  is close to  $\hat{\omega}$ , Eq. (43) is found to be close to  $\pm 1$  with the aid of Eq. (41). Then the first term remains dominant in Eq. (42), accounting for approximately 80% of the total owing to the numerator  $\gamma-1 = 0.24$  in the parentheses.

We assume  $f_{\text{surf}}$  to be a linear function of  $\varphi$ , or  $\psi$ , as usual in studying the PA [32,47]. The surface field  $h$  is defined as the negative of the coefficient of  $\psi$ . This assumption and this definition are involved in calculating the equilibrium profile, which is used in Sec. IV;  $|h|$  represents the strength of the PA and vanishes in its absence. The calculation procedure is mentioned below Eq. (16) and is the same as that of Ref. [47]. Applying Eqs. (37) and (40), we find that  $\hat{\psi}^{(0)}(\hat{r})$  is the solution of

$$0 = \hat{f}'(\hat{\psi}) - \frac{1}{2} \frac{\partial \hat{\omega}^{-\eta\nu}}{\partial \hat{\psi}} (\partial_{\hat{r}} \hat{\psi})^2 - \hat{\omega}^{-\eta\nu} \left( \partial_{\hat{r}}^2 + \frac{1}{\hat{r}} \partial_{\hat{r}} \right) \hat{\psi} \quad \text{for } \hat{r} < 1, \quad (44)$$

together with the boundary condition at the wall,  $(\hat{\psi}^{(0)})'(1) = \hat{h} \hat{\omega}^{\eta\nu}$ , where  $\hat{h}$  is defined as  $h T_* / (T \mu_* r_{\text{tube}})$ . These equations are shown in Appendix D of Ref. [27]. Notably,  $\hat{\psi}^{(0)}$  is totally determined by  $|\hat{\tau}|$  and  $\hat{h}$ , and is changed to its negative when  $\hat{h}$  is changed to its negative. The latter property follows from the parities of  $\hat{\omega}$  and  $\hat{f}$  mentioned below Eq. (41). In particular, when  $h$  vanishes to make the PA absent,  $\psi^{(0)}$  equals  $\psi^{(\text{ref})} = 0$ .

#### D. Formulas incorporating the RLFT

We apply Eqs. (4), (37), and (40) to obtain

$$u^{(0)} - u^{(\text{ref})} = - \frac{(T^{(0)})^2 \mu_* \psi_*}{T_c T_*} \frac{\partial}{\partial \tau} \left( \hat{f} + \frac{\hat{\omega}^{-\eta\nu}}{2} |\partial_{\hat{r}} \hat{\psi}^{(0)}|^2 \right) + \bar{H}_-^{(\text{ref})} \psi^{(0)}, \quad (45)$$

where the partial derivative with respect to  $\tau$  is done with  $\hat{\psi}$  fixed and is evaluated at  $\varepsilon = 0$ . In deriving the second term on the r.h.s. above, we drop one term, which is proportional to the thermal expansion coefficient. This term gives negligibly small contribution to our later numerical results, as described in Appendix F. Owing to Eqs. (8), (37), and (40), we have

$$P^{(0)} - P^{(\text{ref})} = - \frac{\mu_* \psi_* T^{(0)}}{T_*} \left( \hat{f} + \frac{\hat{\omega}^{-\eta\nu}}{2} |\partial_{\hat{r}} \hat{\psi}^{(0)}|^2 \right). \quad (46)$$

We define a scaled thermal force density,  $\hat{\sigma}_z^{(\text{th})}$ , so that Eq. (35) is rewritten as

$$\sigma_z^{(\text{th})}(\hat{r} r_{\text{tube}}) = \frac{\mu_* \psi_* \delta T}{\tau_* T_* L_{\text{tube}}} \hat{\sigma}_z^{(\text{th})}(\hat{r}) \quad (47)$$

and have

$$\hat{\sigma}_z^{(\text{th})} = \tau_* \left( \hat{f} + \frac{1}{2 \hat{\omega}^{\eta\nu}} |\partial_{\hat{r}} \hat{\psi}^{(0)}|^2 \right) + \frac{T^{(0)}}{T_c} \left( \frac{\partial \hat{f}}{\partial \hat{\tau}} - \frac{\eta\nu}{2 \hat{\omega}^{\eta\nu+1}} \frac{\partial \hat{\omega}}{\partial \hat{\tau}} |\partial_{\hat{r}} \hat{\psi}^{(0)}|^2 \right), \quad (48)$$

which is evaluated at  $\varepsilon = 0$ . Equation (48) is determined by  $\hat{\tau}$  and  $\hat{h}$  except for the factors  $\tau_*$  and  $T^{(0)}/T_c$ , and is independent of the sign of  $\hat{h}$ . This independence follows from the parities of  $\hat{\omega}$ ,  $\hat{f}$ , and  $\hat{\psi}^{(0)}$  mentioned at the end of the preceding subsection. The magnitude of the sum in the second parentheses, in particular, is determined by  $|\hat{\tau}|$  and  $|\hat{h}|$  owing to Eqs. (42) and (43).

The independence of Eq. (48) from the sign of  $h$  implies that the thermal force density, and therefore, the direction of thermo-osmosis, are determined irrespective of which component is preferentially adsorbed onto the tube's wall. This property presupposes  $\psi^{(\text{ref})} = 0$  and results from the parities of  $\hat{\omega}$ ,  $\hat{f}$ , and  $\hat{\psi}^{(0)}$ . In deriving Eq. (48), the last term on the r.h.s. of Eq. (45) cancels out the last term in the parentheses of Eq. (35). This last term comes from the thermodynamic force  $-\delta(\mu_-/T)$ , whereas the rest gives the excess enthalpy density. As a result, Eq. (48) becomes even with respect to  $\hat{\psi}^{(0)}$  in the framework of the RLFT, which describes universal properties near the critical point. In particular, the even parity of the free-energy density with respect to the order parameter is inherent to the  $\psi^4$  theory, and should hold universally near the critical point regardless of the approximations made in the derivation of the RLFT.

Equation (36) is rewritten as

$$v_z^{(\text{th})}(\hat{r} r_{\text{tube}}) = \frac{8 T_* \delta T}{T_* \tau_* \pi r_{\text{tube}}^2} \int_{\hat{r}}^1 d\hat{r}_1 \frac{1}{\hat{r}_1 \hat{\eta}(\hat{r}_1)} \int_0^{\hat{r}_1} d\hat{r}_2 \hat{r}_2 \hat{\sigma}_z^{(\text{th})}, \quad (49)$$

TABLE I. Parameter values. Origins of the values are described in the text.

| Mixture | $T_c$ [K] | $\xi_0$ [nm] | $\tau_* \times 10^5$ | $C_2$ [cm <sup>6</sup> /g <sup>2</sup> ] | $\psi_*$ [g/cm <sup>3</sup> ] | $\mu_*$ [cm <sup>2</sup> /s <sup>2</sup> ] | $\eta_*$ [mPa s] |
|---------|-----------|--------------|----------------------|--|-------------------------------|--|------------------|
| LW      | 307       | 0.198        | 5.12                 | 0.714                                    | 0.0470                        | 137  | 2.44             |
| NEMP    | 300       | 0.230        | 6.49                 | 1.05                                     | 0.0419                        | 150  | 0.510            |

whereas the total mass flow rate in thermo-osmosis is given by

$$\frac{d\mathcal{M}_R^{(\text{th})}}{dt} = \frac{\rho^{(\text{ref})}\mathcal{I}_* \delta T}{T_* \tau_*} \Omega[1, \hat{\sigma}_z^{(\text{th})}], \quad (50)$$

which is proportional to  $\delta T$ . The constant of proportionality represents the thermo-osmotic conductance. We define the dimensionless thermo-osmotic conductance, denoted by  $\hat{G}^{(\text{th})}$ , as the quotient of the constant divided by  $\rho^{(\text{ref})}\mathcal{I}_*/(T_* \tau_*)$ , and have

$$\hat{G}^{(\text{th})} = \Omega[1, \hat{\sigma}_z^{(\text{th})}] = 16 \int_0^1 d\hat{r} \hat{r} \hat{v}_z^{(\text{th})}(\hat{r}), \quad (51)$$

where  $\hat{v}_z^{(\text{th})}(\hat{r})$  is defined as the double integral of Eq. (49). If we change the sign of  $\hat{h}$ ,  $\hat{\sigma}_z^{(\text{th})}(\hat{r})$  remains the same. However, it is not the case with  $v_z^{(\text{th})}$  of Eq. (49),  $d\mathcal{M}_R^{(\text{th})}/(dt)$  of Eq. (50), and  $\hat{G}^{(\text{th})}$  of Eq. (51) because  $\hat{\eta}$  is not always an even function of  $\hat{\psi}$ .

Some of the formulas of the Onsager coefficients are simplified using Eqs. (37) and (40). We have  $f''(0) = |\hat{\tau}|^\gamma$  and

$$f''(0) = \frac{k_B T C_2 |\tau|^\gamma}{3u^* \xi_0^3}. \quad (52)$$

Equation (25), where  $\chi$  can be replaced by  $1/f''(\psi)$ , gives

$$\Lambda_* = \frac{3u^* R T_c \xi_0^2 \tau_*^{\nu-\gamma}}{C_2 T_* \eta_*}. \quad (53)$$

Thus, as described in Appendix E of Ref. [27], we have

$$\hat{\Lambda} = \hat{\omega}^{\nu(z_\psi-2)} [f''(\hat{\psi})]^{-1} \quad (54)$$

evaluated at  $\varepsilon = 0$ . In the second terms on the r.h.s.'s of Eqs. (33) and (34), the coefficients outside the integrals are respectively rewritten as

$$\mathcal{I}_* \psi_* T^{(0)} \frac{16\pi T_c}{9T^{(0)}} \quad \text{and} \quad \mathcal{I}_* \mu_* \psi_* T^{(0)} \frac{16\pi T_c}{9T^{(0)}} \quad (55)$$

by using Eq. (25) with  $R = 1/(6\pi)$  and Eq. (54). The integrals can be calculated if  $\hat{H}_-^{(0)}$  can be calculated. To calculate  $\hat{Y}^{(0)}$  contained in the first terms on the r.h.s.'s of Eqs. (32)–(34), we can use Eq. (45), which involves  $\hat{H}_-^{(\text{ref})}$ . Thus, it is necessary to know how  $\hat{H}_-$  depends on  $\rho$  and  $\varphi$  to calculate these integrals and terms. The dependence is given in such a theoretical framework as used in Refs. [61–64].

#### IV. NUMERICAL RESULTS OF THERMO-OSMOSIS

In this section we study thermo-osmosis numerically with the aid of the formulas in Sec. III D and the software *Mathematica* (Wolfram Research), using the material constants of a mixture of 2,6-lutidine and water (LW) near the LC point and a mixture of nitroethane and 3-methylpentane (NEMP) near

the UC point. In each mixture, the former (latter) component is taken to be the component a (b). The tube radius  $r_{\text{tube}}$  is set to 0.1  $\mu\text{m}$ . The parameter values we use are listed in Table I and are the same as used in Ref. [27]. The values of  $\xi_0$  are taken from the experimental data of Refs. [54,65]. The first entry of Eq. (38) gives the values of  $\tau_*$ , which appears in Eq. (48). In Appendix C of Ref. [27], we estimate  $C_2$  from the data of Refs. [66,67]. The second entry of Eq. (38) gives the value of  $\psi_*$ , and then Eq. (28) gives that of  $\mu_*$ . In Appendix E of Ref. [27], we take into account the weak singularity to obtain the viscosity as a function of  $\tau$  and  $\psi$  according to Refs. [68,69], and find the value of  $\eta_*$  from the data of Refs. [65,70–72]. These values give  $\mathcal{I}_* L_{\text{tube}} = 1.04 \times 10^{-2}$  ( $4.84 \times 10^{-2}$ )  $\mu\text{m}^4/\text{s}$  for a mixture of LW (NEMP). The correlation length in the middle of the reservoir in the reference state, given by  $\xi^{(\text{ref})}$ , reflects the thickness of the adsorption layer. To study the total mass flow rate when  $\xi^{(\text{ref})}$  is distinctly larger or smaller than  $r_{\text{tube}}$ , we mainly use  $|\tau| = 1.25 \times 10^{-5}$  and  $3.2 \times 10^{-3}$ , which respectively give  $\xi^{(\text{ref})} \approx 2r_{\text{tube}}$  and  $r_{\text{tube}}/10$ .

We mainly use  $\hat{h} = 73.0$  (66.6) for a mixture of LW (NEMP), which amounts to  $h \approx 0.1 \text{ cm}^3/\text{s}^2$ . This value comes from the following estimation; the value of  $h$  has not been measured experimentally to the best of our knowledge. The minimum of the Leonard-Jones potential between the wall and a component molecule generally differs depending on whether the component is a or b. An estimate of the difference is  $k_B T_c/10$  [73]. We write  $l_{\text{int}}$  for the typical range of the interaction potential. The change in  $\psi$  can be related with the corresponding change in  $n_a - n_b$ , where  $n_j$  denotes the molecule-number density of the component  $j$ . Regarding  $h\psi$  as the deviation of  $(n_a - n_b)k_B T_c l_{\text{int}}/10$  from its value at the critical point, we use  $l_{\text{int}} \approx 0.1 \text{ nm}$  to obtain the above-mentioned value of  $h$ .

#### A. Equilibrium profile and thermal force density

Numerical results of  $\hat{\psi}^{(0)}$  are obtained using the procedure described at the end of Sec. III C and shown in Fig. 2. Because of  $\hat{h} > 0$ ,  $\hat{\psi}^{(0)}(\hat{r})$  increases with  $\hat{r}$ . At  $|\tau| = 3.2 \times 10^{-3}$ , the adsorption layer appears to localize near the tube's wall, and  $\hat{\psi}^{(0)}(\hat{r})$  is larger for a mixture of NEMP than for a mixture of LW in the whole region of  $0 \leq \hat{r} \leq 1$  although the difference can be identified only for some values of  $\hat{r}$  in the figure. This magnitude relationship is reasonable considering that  $|\hat{\tau}|$  is smaller for a mixture of NEMP. The relationship holds only for  $\hat{r} < 0.7$  at  $|\tau| = 1.25 \times 10^{-5}$ , where  $\xi^{(\text{ref})}$  exceeds  $r_{\text{tube}}$ . At this value of  $|\tau|$  and at  $\hat{r} = 0$ , the compositions become definitely off-critical, and the local values of  $\xi$  are approximately reduced to  $r_{\text{tube}}/2$  for both mixtures.

We use  $\hat{\psi}^{(0)}$  for  $\hat{\psi}$  of Eq. (48) to calculate  $\hat{\sigma}_z^{(\text{th})}$  numerically. The results at  $|\tau| = 3.2 \times 10^{-3}$ , shown by circles in the graphs of Fig. 3, distinctly increase in magnitude near



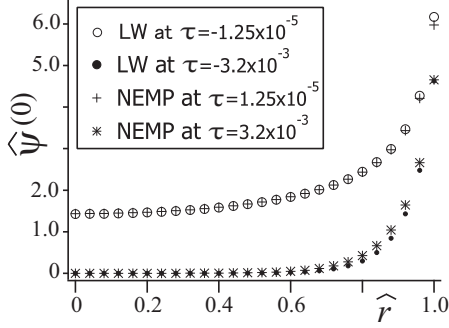


FIG. 2. Plots of the dimensionless order parameter at equilibrium,  $\hat{\psi}^{(0)}(\hat{r})$ , against the dimensionless radial distance  $\hat{r}(\equiv r/r_{\text{tube}})$ . The surface field is set to  $h = 0.1 \text{ cm}^3/\text{s}^2$ . For a mixture of LW (NEMP), open circles (crosses) represent  $\hat{\psi}^{(0)}(\hat{r})$  at  $|\tau| = 1.25 \times 10^{-5}$ , whereas closed circles (asterisks) represent  $\hat{\psi}^{(0)}(\hat{r})$  at  $|\tau| = 3.2 \times 10^{-3}$ . We use the values of  $\tau_*$  in Table I to find  $\hat{\tau} = -0.24$  (0.19) for open circles (crosses) and  $\hat{\tau} = -63$  (49) for closed circles (asterisks).

the wall, similarly to  $\hat{\psi}^{(0)}$  in Fig. 2. Hereafter,  $\tau$  represents the reduced temperature in the reference state. The first term of Eq. (42) contributes to the second term on the r.h.s. of Eq. (48) via the term  $\partial \hat{f}/(\partial \hat{\tau})$ . Crosses in Fig. 3 represent this contribution, which is denoted by  $\hat{\sigma}_z^{(\text{sq})}$  and is given by

$$\hat{\sigma}_z^{(\text{sq})}(\hat{r}) = \pm \frac{T^{(0)}}{2T_c} \hat{\omega}^{\nu-1} \hat{\psi}^2. \quad (56)$$

This is evaluated at  $\varepsilon = 0$  with the same sign as  $\tau$  being taken. This sign for  $\hat{\psi} \neq 0$  comes from that of  $A_0$ , which is negative (positive) for the LC (UC) point. The rest in the second term on the r.h.s. of Eq. (48) is plotted with triangles. The first term on the r.h.s. of Eq. (48), which originates from the scalar-pressure deviation Eq. (46), is plotted with squares. This term gives negligibly small contributions to  $\hat{\sigma}_z^{(\text{th})}$  in the whole region of  $\hat{r}$ . It remains the case as far as we examine for the values of  $|\tau|$  ranging from  $1.25 \times 10^{-5}$  to  $6.4 \times 10^{-3}$  although data are not shown. Near the wall in Fig. 3, we can see that  $\hat{\sigma}_z^{(\text{sq})}(\hat{r})$  is dominant in  $\hat{\sigma}_z^{(\text{th})}(\hat{r})$ , and the ratio  $\hat{\sigma}_z^{(\text{sq})}(\hat{r})/\hat{\sigma}_z^{(\text{th})}(\hat{r})$  at  $\hat{r} = 1$  is 0.86 (0.85)

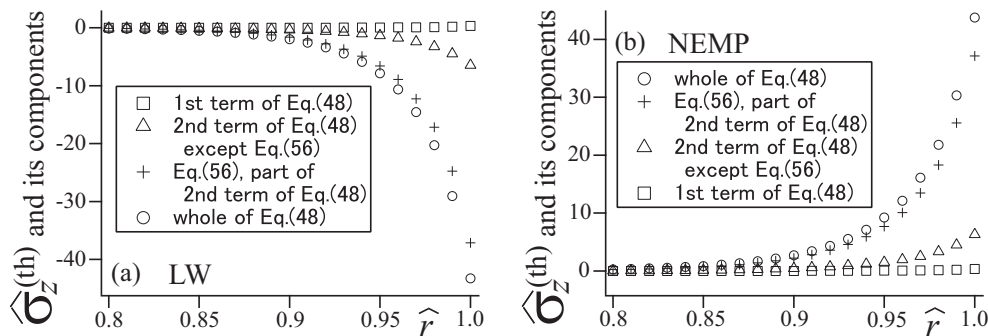


FIG. 3. Plots of the scaled thermal force density,  $\hat{\sigma}_z^{(\text{th})}$ , and its components against the dimensionless radial distance  $\hat{r}(\geq 0.8)$  at  $|\tau| = 3.2 \times 10^{-3}$  for a mixture of LW (a) and a mixture of NEMP (b). Here, the reduced temperature  $\tau$  is evaluated at  $T = T^{(0)}$  and is negative (positive) in the former (latter) mixture. The surface field is set to  $h = 0.1 \text{ cm}^3/\text{s}^2$ . Circles represent  $\hat{\sigma}_z^{(\text{th})}$  of Eq. (48), whereas squares represent its first term. Its second term can be separated into two parts;  $\hat{\sigma}_z^{(\text{sq})}$  of Eq. (56) and the rest. Crosses represent the former, whereas triangles represent the latter. The results continue to approach zero as  $\hat{r}$  decreases to zero, although the results for  $\hat{r} < 0.8$  are not shown here.

for a mixture of LW (NEMP). When  $|\tau|$  is set to  $1.25 \times 10^{-5}$ , the ratio remains approximately the same, 0.88 (0.87), although each of  $\hat{\sigma}_z^{(\text{sq})}(\hat{r})$  and  $\hat{\sigma}_z^{(\text{th})}(\hat{r})$  at  $\hat{r} = 1$  roughly doubles.

In Fig. 4 for a mixture of NEMP,  $\hat{\sigma}_z^{(\text{sq})}(\hat{r})$  and  $\hat{\sigma}_z^{(\text{th})}(\hat{r})$  become larger as  $\tau$  is smaller and  $h$  is larger. For various values of  $|\tau|$  and  $h$  examined in Figs. 3 and 4, over the whole region of  $\hat{r}$ , the ratio  $\hat{\sigma}_z^{(\text{sq})}(\hat{r})/\hat{\sigma}_z^{(\text{th})}(\hat{r})$  remains approximately the same as the ratio at  $\hat{r} = 1$ . Thus, as far as examined,  $\hat{\sigma}_z^{(\text{th})}(\hat{r})$  is negative (positive) for a mixture of LW (NEMP) and is contributed dominantly from  $\hat{\sigma}_z^{(\text{sq})}(\hat{r})$ . In each inset of Fig. 4,  $\hat{\psi}^{(0)}(\hat{r})$  increases more steeply near the wall as  $h$  is larger, similarly to  $\hat{\sigma}_z^{(\text{th})}(\hat{r})$  in the main figure. For each value of  $h$  in Figs. 4(a) and 4(b), as  $\hat{r}$  decreases,  $\hat{\sigma}_z^{(\text{th})}(\hat{r})$  decreases more gradually at the smaller value of  $\tau$ , similarly to  $\hat{\psi}^{(0)}(\hat{r})$ . These similarities can be explained by the dominance of Eq. (56) in  $\hat{\sigma}_z^{(\text{th})}(\hat{r})$ . The dominance of Eq. (56) in the term involving  $\partial \hat{f}/(\partial \tau)$  on the r.h.s. of Eq. (48) is expected from the approximate estimation mentioned below Eq. (43).

## B. Velocity field and conductance

As mentioned in the preceding subsection,  $\hat{\psi}^{(0)}$  is used in calculating  $\hat{\sigma}_z^{(\text{th})}$ , which appears in the double integral of Eq. (49). We numerically calculate the double integral, which gives  $\hat{v}_z^{(\text{th})}(\hat{r})$  as mentioned below Eq. (51), to show the results in Fig. 5. When  $\delta T$  is positive,  $\hat{v}_z^{(\text{th})}$  has the same sign as  $v_z^{(\text{th})}$ . At  $|\tau| = 3.2 \times 10^{-3}$ , it appears that  $\hat{v}_z^{(\text{th})}(\hat{r})$  changes only for  $\hat{r} > 0.8$  to make the velocity slip across a narrow region near the wall. This is because, as shown in Fig. 4(b), the adsorption layer and the thermal force density localize sharply in this region. The dimensionless slip velocity is given by  $\hat{v}_z^{(\text{th})}(0)$ , which is  $-0.042$  (0.061) for a mixture of LW (NEMP) at  $h = 0.1 \text{ cm}^3/\text{s}^2$ . Converting the value to the slip velocity with dimensions, we find it to be  $-7.09$  (38.2)  $(\mu\text{m})^2/(\text{s K})$  multiplied by  $\delta T/L_{\text{tube}}$ , which is comparable in magnitude to typical thermophoretic mobility far from the critical point [8,74–76]. In passing, these values can be evaluated approximately using the Gaussian model mentioned in Appendix G. For each value of  $h$  in

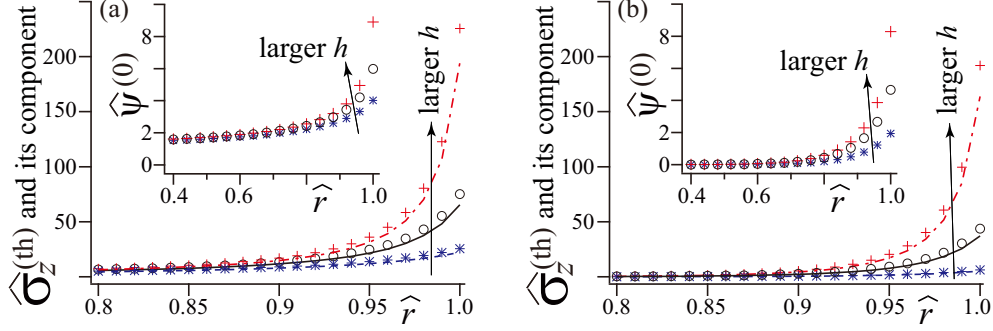


FIG. 4. Plots of the scaled thermal force density,  $\hat{\sigma}_z^{(\text{th})}$ , and its dominant term  $\hat{\sigma}_z^{(\text{sq})}$  against the dimensionless radial distance  $\hat{r} (\geq 0.8)$  for a mixture of NEMP. The reduced temperature  $\tau$  evaluated at  $T = T^{(0)}$  is  $1.25 \times 10^{-5}$  in (a) and  $3.2 \times 10^{-3}$  in (b). The surface field  $h$  is set to  $10^{-1} \text{ cm}^3/\text{s}^2$  for circles ( $\hat{\sigma}_z^{(\text{th})}$ ) and solid curves ( $\hat{\sigma}_z^{(\text{sq})}$ ); these results in (b) are also shown in Fig. 3(b). Setting  $h$  to  $10^{-0.5}$  ( $10^{-1.5}$ )  $\text{cm}^3/\text{s}^2$ , we obtain results shown by red crosses and dash-dot curves (blue asterisks and dashed curves); symbols represent  $\hat{\sigma}_z^{(\text{th})}$  and curves represent  $\hat{\sigma}_z^{(\text{sq})}$ . The change of  $h$  is indicated by arrows. (Insets) Plots of the dimensionless order parameter at equilibrium,  $\hat{\psi}^{(0)}(\hat{r})$ , against  $\hat{r} (\geq 0.4)$ . The parameter values for each symbol are the same as those for the same symbol in the main figure in each of (a) and (b). The results of the circles are also shown in Fig. 2.

Fig. 5,  $|\hat{v}_z^{(\text{th})}(\hat{r})|$  at  $|\tau| = 1.25 \times 10^{-5}$  is larger than  $|\hat{v}_z^{(\text{th})}(\hat{r})|$  at  $|\tau| = 3.2 \times 10^{-3}$  inside the tube and increases gradually in magnitude as  $\hat{r}$  decreases without showing an obvious slip. In Fig. 5(b),  $\hat{v}_z^{(\text{th})}(\hat{r})$  increases with  $h$  inside the tube, as expected. The spatial resolution of our formulation is given by  $\xi$ . For  $h = 0.1 \text{ cm}^3/\text{s}^2$  and  $|\tau| = 1.25 \times 10^{-5}$  ( $3.2 \times 10^{-3}$ ), a mixture of LW has  $\xi/r_{\text{tube}} = 0.030$  (0.036) and a mixture of NEMP has 0.032 (0.038) at  $\hat{r} = 1$ . With the resolution given by these values, one would trace rapid changes of  $\hat{v}_z^{(\text{th})}$  near the wall shown in Fig. 5.

When  $\delta T$  is positive,  $\sigma_z^{(\text{th})}(\hat{r})$  has the same sign as  $\hat{\sigma}_z^{(\text{th})}(\hat{r})$ . For each mixture in our numerical results, the sign of  $\hat{\sigma}_z^{(\text{th})}(\hat{r})$  remains the same for  $0 \leq \hat{r} \leq 1$ , and thus is the same as that of  $\hat{v}_z^{(\text{th})}(\hat{r})$  and that of  $\hat{G}^{(\text{th})}$  of Eq. (51);  $\hat{G}^{(\text{th})} > 0$  ( $< 0$ ) means that the flow direction is the same as (opposite to) the direction of the temperature gradient. Thus, according to our numerical results, a mixture of NEMP near the UC point flows towards the reservoir with the higher temperature, whereas a mixture of LW near the LC point flows in the opposite

direction. The flow direction is determined irrespective of which component is adsorbed onto the tube's wall; the irreversibility comes from the independence of Eq. (48) from the sign of  $h$ .

Logarithmic plots of  $|\hat{G}^{(\text{th})}|$  against  $|\tau|$  are shown in Fig. 6, where  $|\hat{G}^{(\text{th})}|$  increases as  $|\tau|$  decreases. This is because larger susceptibility makes the PA stronger. For smaller values of  $|\tau|$ , the increase becomes more gradual. This would represent effect of the size of the tube, considering that  $\xi^{(\text{ref})}$  exceeds  $r_{\text{tube}}$  approximately for  $|\tau| < 5 \times 10^{-5}$ . Equation (56),  $\hat{\sigma}_z^{(\text{sq})}$ , contributes to  $\hat{G}^{(\text{th})}$  dominantly in the range of  $\tau$  examined in Fig. 6. Changing the value of  $h$  for a mixture of NEMP, we calculate  $\hat{G}^{(\text{th})}$  to show the results in Fig. 7. As  $h$  increases,  $\hat{G}^{(\text{th})}$  increases, as expected since  $\hat{\psi}^{(0)}$ ,  $\hat{\sigma}_z^{(\text{th})}$ , and  $\hat{v}_z^{(\text{th})}$  then increase in Figs. 4 and 5(b). In Fig. 7(b),  $\hat{G}^{(\text{th})}$  becomes less dependent on  $h$  in the logarithmic scale for the smaller value of  $\tau$ . This tendency is also observed for the dependence of  $\hat{v}_z^{(\text{th})}$  on  $h$  in Fig. 5(b). The contribution from  $\hat{\sigma}_z^{(\text{sq})}$  to  $\hat{G}^{(\text{th})}$  remains dominant for the values of  $\tau$  and  $\hat{h}$  examined in Fig. 7(b).

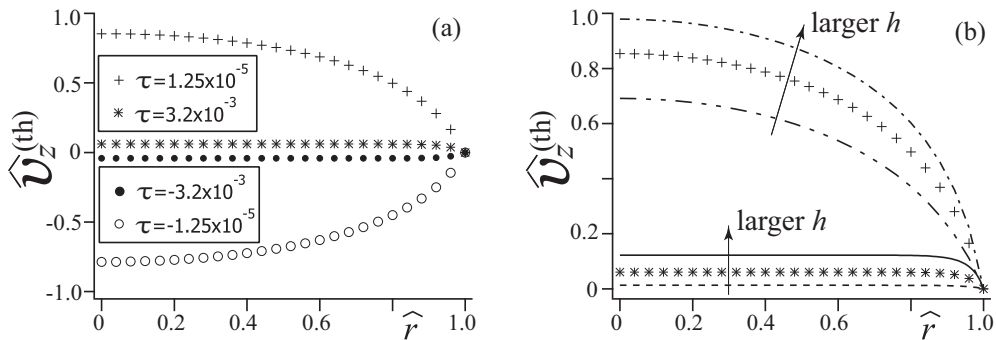


FIG. 5. The  $z$  component of the dimensionless velocity in thermo-osmosis,  $\hat{v}_z^{(\text{th})}(\hat{r})$ , is plotted against the dimensionless radial distance  $\hat{r}$ . (a) Closed and open circles represent  $\hat{v}_z^{(\text{th})}(\hat{r})$  for a mixture of LW at  $\tau = -3.2 \times 10^{-3}$  and  $-1.25 \times 10^{-5}$ , respectively. The reduced temperature  $\tau$  is evaluated at  $T = T^{(0)}$ . Asterisks and crosses represent  $\hat{v}_z^{(\text{th})}(\hat{r})$  for a mixture of NEMP at  $\tau = 3.2 \times 10^{-3}$  and  $1.25 \times 10^{-5}$ , respectively. The surface field is set to  $h = 10^{-1} \text{ cm}^3/\text{s}^2$ . (b) Asterisks and crosses represent the same results as those in (a), respectively. The solid curve (dashed curve) represents  $\hat{v}_z^{(\text{th})}(\hat{r})$  for a mixture of NEMP at  $\tau = 3.2 \times 10^{-3}$  with  $h$  set to  $10^{-0.5}$  ( $10^{-1.5}$ )  $\text{cm}^3/\text{s}^2$ . The dash-dot curve (dash-dot-dot curve) represents  $\hat{v}_z^{(\text{th})}(\hat{r})$  at  $\tau = 1.25 \times 10^{-5}$  with  $h$  set to  $10^{-0.5}$  ( $10^{-1.5}$ )  $\text{cm}^3/\text{s}^2$ . The change of  $h$  is indicated by arrows.

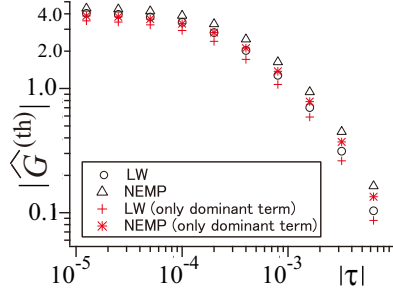


FIG. 6. Logarithmic plots of the absolute value of the dimensionless thermo-osmotic conductance against that of the reduced temperature  $|\tau|$ , evaluated at  $T = T^{(0)}$ , for a mixture of LW (circle) and a mixture of NEMP (triangle) with the surface field set to  $h = 0.1 \text{ cm}^3/\text{s}^2$ . The dimensionless conductance,  $\hat{G}^{(\text{th})} = \Omega[1, \hat{\sigma}_z^{(\text{th})}]$  is negative (positive) for a mixture of LW (NEMP). Red crosses (asterisks) represent  $\Omega[1, \hat{\sigma}_z^{(\text{sq})}]$  for a mixture of LW (NEMP).

### C. Prediction of universal properties

As mentioned below Eq. (56), in our numerical results, the first term on the r.h.s. of Eq. (48) is negligible. This would be mainly because it contains a very small positive factor  $\tau_*$  (Table I). Thus, owing to  $T_c \approx T^{(0)}$ , it is strongly suggested that

$$\hat{\sigma}_z^{(\text{th})} \approx \frac{\partial \hat{f}}{\partial \hat{\tau}} - \frac{\eta\nu}{2\hat{\omega}^{\nu+1}} \frac{\partial \hat{\omega}}{\partial \hat{\tau}} |\partial_{\hat{r}} \hat{\psi}|^2, \quad (57)$$

evaluated at  $\varepsilon = 0$ , holds for any mixture. The r.h.s. above does not presuppose a special mixture because it is determined only by the scaled reduced temperature  $\hat{\tau}$  and the magnitude of the scaled surface field  $|\hat{h}|$ . Using various values of  $(\hat{\tau}, \hat{h})$ , we numerically find that Eq. (56) is dominant in  $\hat{\sigma}_z^{(\text{th})}$ . In this sense, we have

$$\hat{\sigma}_z^{(\text{th})} \approx \pm \frac{\hat{\omega}^{\nu-1}}{2} \hat{\psi}^2 \quad (58)$$

evaluated at  $\varepsilon = 0$ , where the sign is taken as that of  $\tau$ , i.e., as that of  $A_0$  in the bare model. Notably, Eq. (58) is strongly

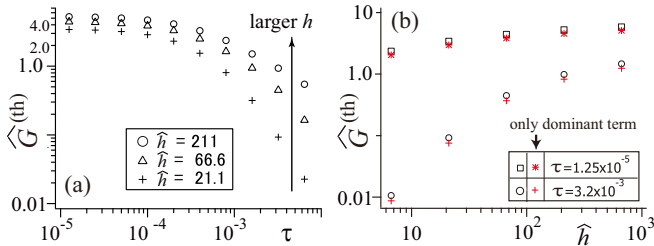


FIG. 7. (a) Logarithmic plots of the dimensionless thermo-osmotic conductance,  $\hat{G}^{(\text{th})}$ , against the reduced temperature  $\tau$ , evaluated at  $T = T^{(0)}$ , for a mixture of NEMP. Triangles here and in Fig. 6 represent the same results with the surface field set to  $h = 10^{-1} \text{ cm}^3/\text{s}^2$ . Circles (crosses) represent  $\hat{G}^{(\text{th})}$  for  $h = 10^{-0.5}$  ( $10^{-1.5}$ )  $\text{cm}^3/\text{s}^2$ . The corresponding values of the scaled surface field  $\hat{h}$  are shown in the figure; the change of  $h$  is indicated by an arrow. (b) Logarithmic plots of  $\hat{G}^{(\text{th})}$  against  $\hat{h}$  for a mixture of NEMP. Squares and circles represent  $\hat{G}^{(\text{th})} = \Omega[1, \hat{\sigma}_z^{(\text{th})}]$  at  $\tau = 1.25 \times 10^{-5}$  and  $3.2 \times 10^{-3}$ , respectively. The values of  $\tau$  are evaluated at  $T = T^{(0)}$ . Red asterisks (crosses) represent  $\Omega[1, \hat{\sigma}_z^{(\text{sq})}]$  at  $\tau = 1.25 \times 10^{-5}$  ( $3.2 \times 10^{-3}$ ).

expected to hold in the critical regime for any mixture, which is also supported by the approximate estimation given below Eq. (43) and by the results in Figs. 6 and 7(b). Therefore, we can predict that, for any mixture near the UC (LC) point, the direction of thermo-osmosis is the same as (opposite to) that of the temperature gradient if the critical composition is kept in the middle of each reservoir, irrespective of which component is adsorbed onto the wall.

### V. FURTHER DISCUSSION AND SUMMARY

Our numerical results are based on the calculation up to the order of  $\varepsilon$ , or in the linear regime with respect to  $\delta T$ . Obviously, as compared with the value of  $\tau$  in the reference equilibrium state, the change in  $\tau$  caused by imposing  $\delta T$  should be sufficiently small in magnitude throughout inside the tube. For example, if  $|\tau|$  is set to  $10^{-3}$  at  $T = T^{(0)}$ , we may set  $|\delta T|/T_c$  to be smaller than its 10%,  $10^{-4}$ . The resultant local changes of  $T$  and  $\hat{\psi}$  shift  $\hat{\sigma}_z^{(\text{th})}$ . As far as examined, although data are not shown, the shift is roughly smaller than 10% in the adsorption layer. For  $|\delta T| = 100 \text{ mK} \ll |T^{(0)} - T_c| \approx 1 \text{ K}$  and  $L_{\text{tube}} = 10 \text{ }\mu\text{m}$ , we find from the results in Fig. 5(a) that the slip velocity is approximately  $0.1 \text{ }\mu\text{m/s}$ , which would be measured experimentally. In passing, in the experiments on the Brownian motion of colloidal particles in a mixture,  $|\tau|$  is set to be smaller than  $10^{-4}$  homogeneously [77,78].

For a mixture in a semi-infinite space bounded by a flat surface, we use Eq. (58) to derive a possible power-law dependence of the slip velocity on  $|\tau|$  in thermo-osmosis, as shown in Appendix G. Thermophoresis would occur for a particle in a mixture in the presence of PA onto the particle surface; the direction of the particle motion is expected to be the same as (opposite to) that of the imposed temperature gradient if the mixture is near the LC (UC) point and has the the critical composition far from the particle. These points clearly require further investigation in future.

The RLFT succeeds in describing several phenomena of a mixture [47]. However, in the theory, crossover to the regular part of the free energy [61–64,79–81] is not considered, the results up to the one-loop order approximation are used, and validity of the definition of the local correlation length in the inhomogeneous composition is not fully discussed. In the present study, the regular parts of the transport coefficients [82] are considered only for the viscosity  $\eta_s$ . In our numerical study,  $f_{\text{surf}}$  is simply regarded as equal to  $-h\psi$  apart from a constant term. These points are to be improved in the future for quantitatively better numerical results on transport properties not only of thermo-osmosis but also of the other phenomena described by the Onsager coefficients. Still, the qualitative property on the flow direction in thermo-osmosis of a mixture should be robust to changes of details in the formulation, considering that it originates from the sign of the coefficient,  $A_0$ , in the bare model.

The pressure-driven transport has attracted much attention, as mentioned in the beginning of Sec. I. For a near-critical mixture in the presence of PA, this transport is numerically studied in Ref. [83]. Claiming that the composition current sensitively depends on the reduced temperature and can be controlled reversibly by either pressure gradient or tempera-

ture, the authors of Ref. [83] suggest potential applications of the transport of a mixture for separation and purification processes. The present study suggests that thermo-osmotic flow is also sensitive to the reference temperature near the critical point and that thermo-osmosis of a mixture may be applied to the processes. Mixture transport driven by multiple thermodynamic forces can also be studied in our framework.

Our present study is summarized as follows. We consider transport of a binary fluid mixture, lying in the one-phase region near the demixing critical point, through a capillary tube. One component is assumed to be adsorbed onto the tube's adiabatic wall and the adsorption layer can be much thicker than the molecular size. Consistently with principles of nonequilibrium thermodynamics, we formulate the hydrodynamics from a coarse-grained free-energy functional using an extended Gibbs-Duhem relation, Eq. (11). The previous derivation of this relation, given in Ref. [45], is generalized in Appendix A to suit the present study. Assuming the critical composition in the middle of each reservoir in the reference equilibrium state, we derive the Onsager coefficients in Sec. III A. In particular, on this assumption, we explicitly derive the formula for the thermal force density, Eq. (35), which is rewritten as Eq. (48) in terms of the renormalized local functional theory [41,47], and predict that, for any binary fluid mixture in the one-phase region near the upper (lower) consolute point, the direction in thermo-osmotic flow is the same as (opposite to) that of the temperature gradient, irrespective of which component is adsorbed onto the tube's wall. The magnitude of the thermo-osmotic conductance increases, with the increase being more gradual owing to the size effect, as the critical point is approached. The thermal force density is given in a scaled form by Eq. (57), which depends only on the scaled reduced-temperature and the scaled surface field, and is dominantly contributed from Eq. (58).

Such mesoscopic inhomogeneity as is generated in a mixture by the surface field can occur in many soft matter systems—polymer solutions, polyelectrolytes, and liquid crystals [39,84]. In particular, their dynamics driven by a temperature gradient would be studied by applying our procedure to a suitable set of hydrodynamic equations based on a coarse-grained free-energy functional. Also, for thermo-osmosis of a solution far from the critical point, our results may help as a guide regarding properties independent of the microscopic details. Hence, our present study would lay solid foundations on nonisothermal hydrodynamics in the presence of mesoscopic inhomogeneity and predict universal properties on thermo-osmosis of a near-critical binary fluid mixture.

#### ACKNOWLEDGMENT

S.Y. was supported by JSPS KAKENHI Grants No. 18K13516 and No. 21K03488.

#### APPENDIX A: NONDISSIPATIVE PART OF THE STRESS TENSOR

For conciseness, we here write  $(T, \rho_n, \nabla \rho_n)$  for the variables of  $f_{\text{bulk}}$  in Eq. (3). Because of Eq. (4),  $s$  and  $u$  also depend on these variables. The entropy density is also a function of  $u$ ,  $\rho_n$ , and  $\nabla \rho_n$ , and we define  $\tilde{s}$  so that

$$s(T, \rho_n, \nabla \rho_n) = \tilde{s}(u(T, \rho_n, \nabla \rho_n), \rho_n, \nabla \rho_n) \quad (\text{A1})$$

holds. Explicit expressions of  $\tilde{s}$ , given in special cases [45,46], are not required in a general argument given below. We have

$$\frac{\partial \tilde{s}}{\partial u} = \frac{1}{T} \quad \text{and} \quad \frac{\partial \tilde{s}}{\partial \zeta} = -\frac{1}{T} \frac{\partial f_{\text{bulk}}}{\partial \zeta} \quad (\text{A2})$$

for  $\zeta = \rho_n$  or  $\nabla \rho_n$ . The coefficients in the quadratic form of  $\nabla \rho_n$  in  $f_{\text{bulk}}$  can depend on  $T$  and  $\rho_n$ . Below, as in Appendix A of Ref. [27], we consider a quasistatic deformation of a mixture to derive Eqs. (9) and (10). We write  $V_t$  for a small region comoving with the deformation. Here,  $t$  is not time but a parameter of the deformation. In general, an infinitesimal change in the entropy is contributed independently from the mechanical work, from the change in the composition, and from the change in the internal energy. Thus, regarding  $T$ ,  $\Pi$ , and  $\mu_n$  as homogeneous over a small region  $V_t$ , we have

$$T \frac{d}{dt} \int_{V_t} d\mathbf{r} \tilde{s} = \Pi : \int_{\partial V_t} dA \mathbf{n}_{\partial V_t} \mathbf{v} - \mu_n \frac{d}{dt} \int_{V_t} d\mathbf{r} \rho_n(\mathbf{r}, t) + \frac{d}{dt} \int_{V_t} d\mathbf{r} u. \quad (\text{A3})$$

Here, the symbol  $:$  is defined so that  $\mathbf{A} : \mathbf{B} = A_{ij} B_{ji}$  holds for two tensors  $\mathbf{A}$  and  $\mathbf{B}$ , and  $\mathbf{n}_{\partial V_t}$  is the outward facing unit normal vector of the surface of  $V_t$ .

Each locus of a mixture is assumed to have each bath of particles and heat. We here write  $\mathbf{j}_n$  and  $\mathbf{j}_u$  for their respective fluxes to the bath, and write  $\mathbf{v}$  for a displacement vector per unit value of  $t$ . The meanings of  $\mathbf{j}_n$  and  $\mathbf{v}$  are different from the ones in the main text, respectively;  $\mathbf{j}_a + \mathbf{j}_b$  does not always vanish here. We can treat  $t$  as the time formally to define the Eulerian time derivative  $\partial/(\partial t)$  and Lagrangian time derivative  $D/(\text{Dt})$ . We have

$$\frac{D\rho_n}{\text{Dt}} = -\rho_n \nabla \cdot \mathbf{v} - \nabla \cdot \mathbf{j}_n \quad \text{and} \quad \frac{Du}{\text{Dt}} = -u \nabla \cdot \mathbf{v} - \nabla \cdot \mathbf{j}_u. \quad (\text{A4})$$

The whole region occupied by the mixture,  $V_{\text{tot}}$ , is deformable here, unlike in the main text. The l.h.s. of Eq. (A3) is rewritten as the integral of  $T[D\tilde{s}/(\text{Dt}) + \tilde{s}\nabla \cdot \mathbf{v}]$  over  $V_t$ . Rewriting the last two terms on the r.h.s. similarly and applying the divergence theorem for the first term, we obtain an equation for the integrands owing to arbitrariness of  $V_t$ . With the aid of this equation, the change in the entropy in  $V_{\text{tot}}$  per unit value of  $t$  is found to be

$$\int_{V_{\text{tot}}} d\mathbf{r} \left[ \frac{D\tilde{s}}{\text{Dt}} + \tilde{s}\nabla \cdot \mathbf{v} \right] = \int_{V_{\text{tot}}} d\mathbf{r} \left[ \frac{\Pi}{T} : \nabla \mathbf{v} + \frac{\mu_n}{T} \nabla \cdot \mathbf{j}_n - \frac{1}{T} \nabla \cdot \mathbf{j}_u \right], \quad (\text{A5})$$

where  $T$ ,  $\Pi$ , and  $\mu_n$  can be inhomogeneous. The factor  $\nabla \cdot \mathbf{v}$  in Eqs. (A4) and (A5) comes from the change rate of the Jacobian between the Eulerian and Lagrangian coordinates. We have

$$\begin{aligned} \frac{D\tilde{s}}{\text{Dt}} &= \frac{\partial \tilde{s}}{\partial u} \frac{Du}{\text{Dt}} + \frac{\partial \tilde{s}}{\partial \rho_n} \frac{D\rho_n}{\text{Dt}} + \frac{\partial \tilde{s}}{\partial (\nabla \rho_n)} \cdot \nabla \left( \frac{D\rho_n}{\text{Dt}} \right) \\ &\quad - \frac{\partial \tilde{s}}{\partial (\nabla \rho_n)} \cdot (\nabla \mathbf{v}) \cdot (\nabla \rho_n), \end{aligned} \quad (\text{A6})$$



which can be rewritten using Eqs. (A2) and (A4). Substituting the result into the l.h.s. of Eq. (A5) and applying integration by parts, we find the l.h.s. to be the sum of

$$-\int_{\partial V_{\text{tot}}} dr \frac{1}{T} \frac{D\rho_n}{Dt} \frac{\partial f_{\text{bulk}}}{\partial(\nabla\rho_n)} \cdot \mathbf{n}_{\partial V_{\text{tot}}} \quad (\text{A7})$$

and the r.h.s. of Eq. (A5) with  $\mu_n$  and  $\Pi$  being replaced by the r.h.s.'s of Eqs. (9) and (10), respectively. Hence, these two equations are derived. Because  $\Pi$  is symmetric, we can derive Eq. (11), or equivalently,  $\nabla \cdot (\Pi/T) = \rho_n \nabla(\mu_n/T) - u \nabla(1/T)$ , which is of the same form as Eq. (2.44) of Ref. [45]. Equation (9) can be used in calculating not only  $\varphi^{(0)}$  but also  $\varphi^{(1)}$ ; the latter need not be obtained in the present study.

We next consider thermodynamics of the mixture in a thin interfacial region regarded as  $\partial V_{\text{tot}}$ . The free energy per unit area of this region is denoted by  $f_{\text{surf}}$  in Eq. (3) and is here denoted by  $f^{(s)}$ . The superscript (s) in general indicates a thermodynamic quantity in  $\partial V_{\text{tot}}$ ; a density with the superscript represents a quantity per unit area. As in Eq. (4), we can introduce internal energy  $u^{(s)}$  and entropy  $s^{(s)}$  using  $f^{(s)}$ . These three quantities are functions of  $T^{(s)}$  and  $\rho_n^{(s)}$ . As Eq. (A3) yields Eq. (A5), an equation for a small comoving area on  $\partial V_{\text{tot}}$  yields an equation representing the change of the entropy on  $\partial V_{\text{tot}}$ . Two points are to be noted in this derivation. First, the mechanical contribution consists of a term involving the two-dimensional pressure tensor  $\Pi^{(s)}$  and a term involving the force normal to the small area. Because  $f^{(s)}$  includes no gradients of mass densities, the pressure tensor is written as the two-dimensional scalar pressure multiplied by the identity tensor on  $\partial V_{\text{tot}}$ . The scalar pressure is denoted by  $P^{(s)}$ . We define  $P_{\perp}^{(s)}$  so that the normal force is  $P_{\perp}^{(s)} \mathbf{n}_{\partial V_{\text{tot}}}$  per unit area. Second, the factor coming from the change rate of the Jacobian is  $\nabla \cdot \mathbf{v}_{\parallel} - 2H_m \mathbf{v} \cdot \mathbf{n}_{\partial V_{\text{tot}}}$ , where  $\mathbf{v}_{\parallel}$  is the projection of  $\mathbf{v}$  on the plane tangential to  $\partial V_{\text{tot}}$ ,  $\nabla \cdot \mathbf{v}_{\parallel}$  indicates the divergence defined on  $\partial V_{\text{tot}}$ , and  $H_m$  denotes the mean curvature of  $\partial V_{\text{tot}}$  [85]. The curvature is defined so that it is positive when the center of curvature lies on the side directed by  $\mathbf{n}_{\partial V_{\text{tot}}}$ .

The temperature at a local area on  $\partial V_{\text{tot}}$ ,  $T^{(s)}$ , should be equal to  $T$  at its adjacent local region of  $V_{\text{tot}}$ . Similarly,  $\rho_n^{(s)}$  is determined by  $\rho_n$  at the adjacent region so that the former equals the latter multiplied by the interfacial region's width. No other factor is involved in determining  $\rho_n^{(s)}$ , which means  $\mu_n^{(s)} = 0$ . Through these relationships,  $f_{\text{surf}}(T, \rho_n)$  equals  $f^{(s)}(T^{(s)}, \rho_n^{(s)})$ . Taking Eq. (A7) into account, we find

$$0 = \frac{\partial f_{\text{surf}}}{\partial \rho_n} + \frac{\partial f_{\text{bulk}}}{\partial(\nabla\rho_n)} \cdot \mathbf{n}_{\partial V_{\text{tot}}} \quad \text{at } \partial V_{\text{tot}} \quad (\text{A8})$$

from the equation representing the change of the entropy on  $\partial V_{\text{tot}}$ . We also find  $P^{(s)} = -f_{\text{surf}}$ , which gives the Laplace pressure  $P_{\perp}^{(s)} = -2f_{\text{surf}}H_m$  [86]. Notably,  $f_{\text{surf}}$  equals the grand-potential density of  $\partial V_{\text{tot}}$  owing to  $\mu_n^{(s)} = 0$ . We need not consider these interfacial forces in calculating the velocity field in the tube. The force exerted on the mixture by the tube's wall is determined so that the no-slip condition is realized.

## APPENDIX B: ONSAGER COEFFICIENTS AND RECIPROCAL RELATIONS

We first consider entropy fluctuations of an equilibrium mixture in the isolated container with the pistons fixed

(Fig. 1). Neglecting the contribution from the mixture in the tube, we can regard the total entropy of the mixture in the container, denoted by  $S$ , as a function of  $\mathcal{M}_{\text{aR}}$ ,  $\mathcal{M}_{\text{bR}}$ , and  $\mathcal{U}_{\text{R}}$ . We have

$$\frac{dS}{dt} = \frac{d\mathcal{U}_{\text{R}}}{dt} \delta\left(\frac{1}{T}\right) + \frac{d\mathcal{M}_{\text{nR}}}{dt} \delta\left(\frac{-\mu_n}{T}\right) \quad (\text{B1})$$

holds up to the second order of the magnitudes of the deviations, with repeated indices being summed up. Equation (B1) is included in Eq. (XV-55) of Ref. [48]. The thermodynamic fluxes are given by the time derivatives on the r.h.s. and are driven by the conjugate thermodynamic forces,  $\delta(1/T)$  and  $-\delta(\mu_n/T)$ . They are respectively the partial derivatives of  $S$  with respect to  $\mathcal{U}_{\text{R}}$  and  $\mathcal{M}_{\text{nR}}$  [49]. We apply the GD relation to obtain

$$\begin{bmatrix} -\delta(P/T) \\ -\delta(\mu_{-}/T) \\ \delta(1/T) \end{bmatrix} = \begin{bmatrix} \rho_{\text{a}}^{(\text{ref})} & \rho_{\text{b}}^{(\text{ref})} & u^{(\text{ref})} \\ 1/2 & -1/2 & 0 \\ 0 & 0 & 1 \end{bmatrix} \begin{bmatrix} -\delta(\mu_{\text{a}}/T) \\ -\delta(\mu_{\text{b}}/T) \\ \delta(1/T) \end{bmatrix}. \quad (\text{B2})$$

The l.h.s. above gives a new set of thermodynamic forces, which is considered in Sec. II B. The transpose of the inverse of the  $3 \times 3$  matrix above equals the  $3 \times 3$  matrix in Eq. (12).

We consider two sets of flow fields, each being driven by the thermodynamic forces  $(-\delta(P/T)_k, -\delta(\mu_{-}/T)_k, \delta(1/T)_k)$ , with  $k$  being i or ii. The resultant thermodynamic fluxes and fields in the tube are also indicated by the subscript  $k$ . Different ways of applying the divergence theorem to the volume integral of  $\eta_{\text{s}}^{(0)} E_{\text{i}}^{(1)} : E_{\text{ii}}^{(1)}$  over the tube interior, denoted by  $V_{\text{tube}}$ , give

$$\int_{V_{\text{tube}}} dr \mathbf{v}_{\text{ii}}^{(1)} \cdot [\nabla \cdot (\eta_{\text{s}}^{(0)} E_{\text{i}}^{(1)})] = \int_{V_{\text{tube}}} dr \mathbf{v}_{\text{i}}^{(1)} \cdot [\nabla \cdot (\eta_{\text{s}}^{(0)} E_{\text{ii}}^{(1)})] \quad (\text{B3})$$

with the aid of Eq. (17) and the no-slip condition at the tube's wall. Here, we neglect effects of the tube's edges on the laminar flow. Substituting Eq. (20) into Eq. (B3), we find that

$$\int_{S_{\text{tube}}} dA \mathbf{v}_{\text{ii},z}^{(1)} \left[ \frac{\rho^{(0)}}{\rho^{(\text{ref})}} \delta\left(\frac{P}{T}\right)_{\text{i}} + \left(\varphi^{(0)} - \frac{\varphi^{(\text{ref})}}{\rho^{(\text{ref})}}\right) \delta\left(\frac{\mu_{-}}{T}\right)_{\text{i}} - \left(P^{(0)} + u^{(0)} - \frac{\rho^{(0)} u^{(\text{ref})}}{\rho^{(\text{ref})}}\right) \delta\left(\frac{1}{T}\right)_{\text{i}} \right] \quad (\text{B4})$$

equals the above equation with the subscripts i and ii exchanged. Putting  $\delta(P/T)_{\text{i}}$ ,  $\delta(\mu_{-}/T)_{\text{i}}$ ,  $\delta(P/T)_{\text{ii}}$ , and  $\delta(1/T)_{\text{ii}}$  equal to zero, we use Eqs. (21)–(24) to find  $L_{23} = L_{32}$ . Likewise, we can obtain  $L_{13} = L_{31}$  by putting  $\delta(P/T)_{\text{i}}$ ,  $\delta(\mu_{-}/T)_{\text{i}}$ ,  $\delta(\mu_{-}/T)_{\text{ii}}$ , and  $\delta(1/T)_{\text{ii}}$  equal to zero. The other reciprocal relations can be derived similarly, as shown in Appendix B of Ref. [27].

## APPENDIX C: CALCULATION OF THE FIELDS IN THE TUBE

We rewrite the l.h.s. of Eq. (6) as  $\varepsilon$  multiplied by

$$2\nabla \cdot (\eta_{\text{s}}^{(0)} \mathbf{E}^{(1)}) = \nabla \cdot \{ \eta_{\text{s}}^{(0)} [\nabla \mathbf{v}^{(1)} + (\nabla \mathbf{v}^{(1)})^{\text{T}}] \}. \quad (\text{C1})$$

With the aid of Eq. (11), we rewrite the r.h.s. of Eq. (6) as  $\varepsilon$  multiplied by

$$\begin{aligned} \nabla \cdot \Pi^{(1)} = & \rho_n^{(0)} \nabla \mu_n^{(1)} + s^{(0)} \nabla T^{(1)} \\ & + \frac{\nabla T^{(1)}}{T^{(0)}} \cdot \frac{\partial f_{\text{bulk}}}{\partial (\nabla \rho_n)} (\nabla \rho_n^{(0)}), \end{aligned} \quad (\text{C2})$$

where the partial derivative of  $f_{\text{bulk}}$  is evaluated at  $\varepsilon = 0$ . Thus, the  $x$  and  $y$  components of Eq. (6) give

$$0 = \rho^{(0)} \bar{\nabla} \mu_+^{(1)} + \varphi^{(0)} \bar{\nabla} \mu_-^{(1)} + s^{(0)} \bar{\nabla} T^{(1)}. \quad (\text{C3})$$

Because  $P^{(0)}$ ,  $\rho_n^{(0)}$ , and  $u^{(0)}$  are independent of  $z$ , we obtain

$$\nabla \cdot \mathbf{j}^{(1)} = 0 \quad \text{and} \quad \nabla \cdot \mathbf{j}_q^{(1)} = 0. \quad (\text{C4})$$

The first entry comes from Eqs. (7) and (17), and the second comes from Eqs. (10), (11), and (18). The components of  $\mathbf{j}$  and  $\mathbf{j}_q$  normal to the tube's wall vanish at the impermeable and adiabatic wall. These conditions, the conditions at the tube's edges mentioned in the beginning of Sec. II C, Eq. (C3), and Eq. (C4) are satisfied if  $\mu_n^{(1)}$  and  $T^{(1)}$  are linear functions of  $z$  and are independent of  $x$  and  $y$ . Then,  $\mathbf{j}^{(1)}$  and  $\mathbf{j}_q^{(1)}$  have only  $z$  components and are independent of  $z$ , considering Eq. (19) up to the order of  $\varepsilon$ . With the aid of Eqs. (C1) and (C2), the  $z$  component of Eq. (6) give

$$\bar{\nabla} \cdot (\eta_s^{(0)} \bar{\nabla} v_z^{(1)}) = \rho_n^{(0)} \partial_z \mu_n^{(1)} + s^{(0)} \partial_z T^{(1)}. \quad (\text{C5})$$

The derivatives on the r.h.s. above are constants determined by the thermodynamic forces in Eq. (13). We obtain

$$\begin{aligned} \varepsilon \partial_z T^{(1)} = & -\frac{T^{(0)2}}{L_{\text{tube}}} \delta \left( \frac{1}{T} \right), \\ \varepsilon \partial_z \mu_-^{(1)} = & \frac{T^{(0)}}{L_{\text{tube}}} \left[ \delta \left( \frac{\mu_-}{T} \right) - \mu_-^{(0)} \delta \left( \frac{1}{T} \right) \right], \end{aligned} \quad (\text{C6})$$

and

$$\varepsilon \partial_z \mu_+^{(1)} = \frac{1}{\rho^{(\text{ref})} L_{\text{tube}}} (\delta P - \varphi^{(\text{ref})} \delta \mu_- - s^{(\text{ref})} \delta T), \quad (\text{C7})$$

with the aid of Eq. (15). Thus, we use Eqs. (4) and (8) to rewrite Eq. (C5) as Eq. (20).

Under the specifications mentioned in the preface of Sec. III, Eq. (20) gives

$$\begin{aligned} \varepsilon v_z^{(1)}(r) = & \int_r^{r_{\text{tube}}} dr_1 \frac{1}{r_1 \eta_s^{(0)}(r_1)} \int_0^{r_1} dr_2 r_2 \\ & \times \frac{T^{(0)}}{L_{\text{tube}}} \left[ \delta \left( \frac{-P}{T} \right) + \psi^{(0)}(r_2) \delta \left( \frac{-\mu_-}{T} \right) \right. \\ & \left. + (u^{(0)}(r_2) - u^{(\text{ref})} + P^{(0)}(r_2)) \delta \left( \frac{1}{T} \right) \right]. \end{aligned} \quad (\text{C8})$$

Substituting Eqs. (21) and (C8) into Eqs. (23) and (24) yields

$$L_{11} = \frac{\mathcal{I}_* T^{(0)}}{\mu_* \psi_*} \Omega[1, 1], \quad L_{12} = L_{21} = \frac{\mathcal{I}_* T^{(0)}}{\mu_*} \Omega[1, \hat{\psi}^{(0)}], \quad (\text{C9})$$

and

$$L_{22} = \frac{\mathcal{I}_* \psi_* T^{(0)}}{\mu_*} \Omega[\hat{\psi}^{(0)}, \hat{\psi}^{(0)}] + 2\pi r_{\text{tube}}^2 \frac{\Lambda_* T_*}{L_{\text{tube}}} \int_0^1 d\hat{r} \hat{r} \hat{\Lambda}(\hat{r}). \quad (\text{C10})$$

The other components are given by Eqs. (32)–(34). The factor outside the integral of the second term on the r.h.s. of Eq. (C10) equals  $16\pi T_c \mathcal{I}_* \psi_*/(9\mu_*)$  if we use Eq. (25) with  $R = 1/(6\pi)$  and Eq. (54), as mentioned in Ref. [27].

Setting  $\delta P = \delta c_a = 0$ , we use Eqs. (12)–(14) and (26) to obtain  $d\mathcal{M}_{nR}^{(\text{th})}/(dt)$  as

$$\begin{aligned} & \frac{\delta T}{(T^{(0)})^2} \left[ \rho_n^{(\text{ref})} (P^{(\text{ref})} L_{11} + \bar{H}_-^{(\text{ref})} L_{12} - L_{13}) \right. \\ & \left. \pm \frac{1}{2} (P^{(\text{ref})} L_{21} + \bar{H}_-^{(\text{ref})} L_{22} - L_{23}) \right], \end{aligned} \quad (\text{C11})$$

where the upper (lower) sign is taken for  $n = a$  (b) in the double sign. The sum of Eq. (C11) over  $n = a$  and b gives  $d\mathcal{M}_R^{(\text{th})}/(dt)$ . Rewriting the resultant sum with the aid of Eqs. (32) and (C9), we obtain the same expression of  $d\mathcal{M}_R^{(\text{th})}/(dt)$  as derived in the way mentioned in Sec. III B. The last term in the parentheses of Eq. (35) involves  $L_{12}$ , which is also involved in the diffusio-osmotic conductance calculated in Ref. [27].

#### APPENDIX D: DISSIPATIVE FLUXES

In an equilibrium mixture, we consider a region where the mass densities are homogeneous. There,  $f_{\text{bulk}}$  is a function of  $T$ ,  $\rho$ , and  $\varphi$ , and we have

$$\left( \frac{\partial \mu_-}{\partial \varphi} \right)_{T,P} = \left( \frac{\partial \mu_-}{\partial \varphi} \right)_{T,\rho} + \left( \frac{\partial \mu_-}{\partial \rho} \right)_{T,\varphi} \left( \frac{\partial \rho}{\partial \varphi} \right)_{T,P}. \quad (\text{D1})$$

The first partial derivative of the second term on the r.h.s. above equals  $\partial^2 f_{\text{bulk}}/(\partial \rho \partial \varphi)$ , which vanishes because Eq. (37) is assumed. The second derivative does not diverge, as mentioned in Appendix E. Thus, whether  $T$  and  $P$  are fixed or  $T$  and  $\rho$  are fixed,  $\partial \mu_-/(\partial \varphi)$  is the same, being equal to the inverse of  $\chi$ , which appears in Eq. (25). We have

$$\frac{1}{\chi} = \left( \frac{\partial \mu_-}{\partial c_a} \right)_{T,P} \left( \frac{\partial c_a}{\partial \varphi} \right)_{T,P} = \frac{1}{2\rho^2 \bar{v}_+} \left( \frac{\partial \mu_-}{\partial c_a} \right)_{T,P}, \quad (\text{D2})$$

where  $\bar{v}_+$  denotes  $(\bar{v}_a + \bar{v}_b)/2$ . The second equality above comes from Eq. (34) of Ref. [27]. Because a mixture we consider has  $\rho \bar{v}_+ \approx 1$  [27], Eq. (25) is consistent with the result in Refs. [55,87].

With  $\bar{\delta}$  indicating the deviation from the average, the thermodynamic forces are  $\bar{\delta}(1/T)$ ,  $-\bar{\delta}(\mu_+/T)$ , and  $-\bar{\delta}(\mu_-/T)$  in Eq. (19). This equation is rewritten as

$$\begin{aligned} \mathbf{j} = & -4\bar{\alpha} \nabla \mu_- + 2\bar{\beta} \nabla T \quad \text{and} \\ \mathbf{j}_q - \mu_- \mathbf{j} = & 2T \bar{\beta} \nabla \mu_- - \bar{\gamma} \nabla T, \end{aligned} \quad (\text{D3})$$

whereby  $\bar{\alpha}$ ,  $\bar{\beta}$ , and  $\bar{\gamma}$  are defined. We write  $\check{s} (\equiv s/\rho)$  for entropy per unit mass. As can be seen from Ref. [88], the irreversible fluxes of  $c_a$  and  $\check{s}$  are respectively given by the quotient of the first entry in Eq. (D3) divided by  $2\rho$  and that of the second divided by  $\rho T$ , whereas the conjugate thermodynamic forces are respectively given by  $-2\rho(\delta \mu_-)/T$  and  $-\rho(\delta T)/T$ . After the division, the second term on the r.h.s. of the second entry becomes equal to the product of  $-\rho(\nabla T)/T$  multiplied by  $\bar{\gamma}/\rho^2$ , which is one of the Onsager coefficients. The other coefficients can be similarly obtained. Comparing

Eq. (19) with (D3), we obtain

$$\begin{aligned}\Lambda &= 4\tilde{\alpha}, \quad \kappa = 2T(2\mu_-\tilde{\alpha} - T\tilde{\beta}), \quad \text{and} \\ \lambda &= 4\mu_-T(\mu_-\tilde{\alpha} - T\tilde{\beta}) + T^2\tilde{\gamma}.\end{aligned}\quad (\text{D4})$$

In Refs. [55,87,89], the singular parts of  $\tilde{\alpha}$ ,  $\tilde{\beta}$ , and  $\tilde{\gamma}$ , indicated by the subscript  $\text{sing}$ , are shown to satisfy

$$\frac{\tilde{\beta}_{\text{sing}}}{2\tilde{\alpha}_{\text{sing}}} = -\left(\frac{\partial c_a}{\partial T}\right)_{P,\mu_-} \left(\frac{\partial \mu_-}{\partial c_a}\right)_{T,P} = -\bar{s}_-, \quad (\text{D5})$$

whose second equality comes from Eq. (1), and

$$\frac{\tilde{\gamma}_{\text{sing}}}{4\tilde{\alpha}_{\text{sing}}} = \frac{\rho T}{\chi} \left(\frac{\partial \tilde{s}}{\partial T}\right)_{P,\mu_-} \approx T\bar{s}_-^2. \quad (\text{D6})$$

The approximate equality of Eq. (D6) is explained in the next paragraph. Because of the singular properties of  $\tilde{\alpha}$  and  $\tilde{\beta}$ , the Ludwig-Soret effect has universal properties in a near-critical binary fluid mixture [55,82,87,90–92]. Equations (D4)–(D6) yield Eq. (27). It is to be noted that this equation leads to neglect of the thermal conductivity not exhibiting the critical enhancement [87].

The partial derivative in Eq. (D6) equals

$$\left(\frac{\partial \tilde{s}}{\partial T}\right)_{P,c_a} + \left(\frac{\partial \tilde{s}}{\partial c_a}\right)_{T,P} \left(\frac{\partial c_a}{\partial T}\right)_{P,\mu_-} = \frac{c_P}{\rho T} + 2\bar{s}_- \left(\frac{\partial c_a}{\partial T}\right)_{P,\mu_-}, \quad (\text{D7})$$

where  $c_P$  denotes the isobaric specific heat under constant  $c_a$ . The equality between the second terms on both sides above comes from a Maxwell relation and Eq. (1). The second partial derivative in Eq. (D5) can be rewritten using Eq. (34) of Ref. [27]. As a result, the last partial derivative in Eq. (D7) equals  $\bar{s}_-\chi/(2\rho^2\bar{v}_+)$ . As mentioned in Appendix E,  $c_P$  diverges more weakly than  $\chi$  in the critical regime, where the approximate equality in Eq. (D6) is valid.

An alternative explanation is as follows. In the mode-coupling theory, the singular part of an Onsager coefficient is calculated in terms of the time integral of the two-time correlation function of the reversible fluxes, as mentioned in Sec. 6.5 of Ref. [39]. The Onsager coefficients mentioned above Eq. (D4) are found to be  $\tilde{\gamma}/\rho^2$ ,  $-\tilde{\beta}T/\rho^2$ , and  $\tilde{\alpha}T/\rho^2$ , and their singular parts are linked with the autocorrelation of  $(\delta\tilde{s})\mathbf{v}$ , the cross-correlation of  $(\delta\tilde{s})\mathbf{v}$  and  $(\delta\bar{c}_a)\mathbf{v}$ , and the autocorrelation of  $(\delta\bar{c}_a)\mathbf{v}$ , respectively. This means that, in the critical regime, the ratio of  $\tilde{\gamma}_{\text{sing}}$  to  $-\tilde{\beta}_{\text{sing}}T$  and that of  $-\tilde{\beta}_{\text{sing}}T$  to  $\tilde{\alpha}_{\text{sing}}T$  are given by  $\partial\tilde{s}/(\partial c_a)$  with  $T$  and  $P$  fixed, which is consistent with Eqs. (D5) and (D6).

#### APPENDIX E: INTERNAL-ENERGY FLUCTUATIONS AND APPROXIMATE INCOMPRESSIBILITY

We define  $\mathcal{H}$  as the effective Hamiltonian in the bare model so that the equilibrium probability density functional (EPDF) of  $\rho$  and  $\psi$  is proportional to  $e^{-\mathcal{H}}$ , without the contribution from  $\partial V_{\text{tot}}$  taken into account. As mentioned in Sec. III C,  $\mathcal{H}$  includes the  $\psi^4$  model,

$$\int_{V_{\text{tot}}} d\mathbf{r} \left[ \frac{1}{2}A_0\tau\psi^2 + \frac{\lambda_0}{4!}\psi^4 + \frac{a_0^2}{2}|\nabla\psi|^2 \right], \quad (\text{E1})$$

where  $\lambda_0(>0)$  and  $a_0$  are constants, and the integrand above becomes a part of Eq. (37) divided by  $k_B T$  after coarse

grained. The value of  $T_c$  in the definition of  $\tau$  depends on the stage of the coarse graining. Writing  $m$  for  $(u - u_c)/(k_B T_c)$ , we can also consider the EPDF of  $\rho$ ,  $\psi$ , and  $m$ . We define  $\mathcal{H}_s$  so that this EPDF is proportional to  $e^{-\mathcal{H}_s}$  in the bare model. Integrating out  $m$  from this EPDF should yield the EPDF of  $\rho$  and  $\psi$ . In other words, the latter's Legendre transform is the former, and vice versa. Thus, owing to a term  $A_0\tau\psi^2/2$  in  $\mathcal{H}$ ,  $\mathcal{H}_s$  has a term proportional to  $m\psi^2$  and  $\mathcal{H}$  has a term proportional to  $\tau^2$  [39,60]. We define  $C_0$  so that this term equals  $-C_0\tau^2/(2k_B)$ , and the variance of  $m$  is proportional to  $C_0$ . Coarse graining the  $\psi^4$  model and imposing the self-consistent condition for off-critical compositions set up the RLFT [47]. We can also set it up by coarse graining  $\mathcal{H}_s$ , imposing a self-consistent condition, and integrating out  $m$ . In this procedure,  $C_0$  becomes  $C$  of Eq. (37) because fluctuations of  $m$  are affected by those of  $\psi$  via their coupling term [39,60]. Instead of using Eq. (37) as it is, we can calculate  $\hat{\sigma}^{(\text{th})}$  by evaluating the dependence of  $C$  on  $\xi$  locally. Although data are not shown, the resultant changes from the results of Fig. 3 are negligibly small [64].

The isochoric specific heat  $c_V$ , given by  $-T\partial^2 f_{\text{bulk}}/(\partial T^2)$  with  $\rho$  and  $\varphi$  being fixed, remains finite at the critical point, although it appears to diverge in the regime accessible to usual experiments [39,93]. Linked with the fluctuations of  $m$ , the isobaric specific heat  $c_P$  becomes proportional to  $C$  ( $\propto |\tau|^{-\alpha}$  with  $\alpha = 0.11$ ) in the critical regime with  $c_a = c_{\text{ac}}$  kept [39,94]. The same power-law dependence is shared by the isothermal compressibility  $\kappa_T$  and the thermal expansion coefficient  $\alpha_P$ , which are given by

$$\begin{aligned}\kappa_T &= \frac{1}{\rho} \left(\frac{\partial \rho}{\partial P}\right)_{T,c_a} \quad \text{and} \\ \alpha_P &= -\frac{1}{\rho} \left(\frac{\partial \rho}{\partial T}\right)_{P,c_a} = \kappa_T \left(\frac{\partial P}{\partial T}\right)_{\rho,c_a}.\end{aligned}\quad (\text{E2})$$

These quantities are related with each other via  $\kappa_T(c_P - c_V) = \alpha_P^2 T$ . The singularity of  $\kappa_T$  is generated by coupling between  $\rho - \rho_c$  and  $\psi^2$  in the  $\rho$ -dependent part in the EDPF. We neglect this coupling in Eq. (37), considering that the singularity is not accessible to usual experiments [39,95]. Observed values of  $\kappa_T$  and  $\alpha_P$  are typically  $10^{-9} \text{ Pa}^{-1}$  and  $10^{-3} \text{ K}^{-1}$ , respectively, near the critical point [95,96].

In this paragraph, we show that the last partial derivative of Eq. (D1) is finite. In the region mentioned at the beginning of Appendix D, we simply write  $f$  for  $f_{\text{bulk}}$  and refer to its derivatives by adding subscripts. For example,  $f_{\rho\varphi}$  represents  $\partial^2 f_{\text{bulk}}/(\partial \rho \partial \varphi)$ , which vanishes because of Eq. (37). We have

$$\delta P = \rho(f_{\rho\rho}\delta\rho + f_{\rho T}\delta T) + \varphi(f_{\varphi\varphi}\delta\varphi + f_{\varphi T}\delta T) + s\delta T \quad (\text{E3})$$

owing to Eq. (15). Here, unlike in the main text,  $\delta$  indicates an infinitesimal change. Using Eq. (E3) and  $\varphi = \rho(2c_a - 1)$ , we find  $\delta\varphi$  ( $\delta\rho$ ) equal to  $\varphi$  ( $\rho$ ) multiplied by

$$\delta P \frac{1}{\rho^2 f_{\rho\rho} + \varphi^2 f_{\varphi\varphi}} \quad (\text{E4})$$

when  $T$  and  $c_a$  are fixed. The fraction is found to equal  $\kappa_T$  because of the first entry of Eq. (E2) and Eq. (E3). Considering that the sum in the first (second) parentheses of Eq. (E3) equals  $\delta\mu_+$  ( $\delta\mu_-$ ), we use Eq. (E4) to find that the first entries of Eqs. (1) and (2) give  $\bar{v}_- = \varphi f_{\varphi\varphi} \kappa_T$  and  $\bar{v}_+ = \rho f_{\rho\rho} \kappa_T$ .

Thus, we use Eq. (E3) to find that the last partial derivative in Eq. (D1) equals  $-\bar{v}_-/ \bar{v}_+$ , which result can be derived if  $f_{\rho\varphi}$  does not vanish. At the critical point, this fraction can be written in terms of  $\rho_c$  and  $\varphi_c$  and is finite.

For the following reason, we can use  $\rho_c$  approximately for  $\rho^{(\text{ref})}$ , which appears in Eq. (50) and is involved in returning the dimension to  $\hat{G}^{(\text{th})}$ . For definiteness, we here write  $\tau^{(\text{ref})}$  for the value of  $\tau$  in the reference state. At the state we reach by changing  $\tau$  from zero to  $\tau^{(\text{ref})}$  with  $P$  and  $c_a$  being fixed, how  $\rho$  changes from  $\rho_c$  can be approximately calculated from the regular part of  $\alpha_P$  [95]. The difference between the value of  $\rho$  at this state and  $\rho^{(\text{ref})}$  can be calculated using the last partial derivative in Eq. (D1). Thus, the ratio  $(\rho^{(\text{ref})} - \rho_c)/\rho_c$  is found to be smaller in magnitude than  $10^{-3}$  for  $\tau^{(\text{ref})} = 1/300$ .

#### APPENDIX F: APPROXIMATION IN THE DERIVATION OF EQ. (45)

By using Eq. (E3) to calculate the second entry of Eq. (1), we obtain  $\bar{s}_- = \varphi f_{\varphi\varphi} \alpha_P - f_{\varphi T}$ . The term  $\mu_-^{(\text{ref})} \varphi$  is included in  $f_-$ , as shown in Eq. (40). Its contribution to the second entry of Eq. (4) is

$$-T^2 \left( \frac{\partial}{\partial T} \right)_{\rho, \varphi} \frac{\mu_-^{(\text{ref})} \varphi}{T} = \mu_-^{(\text{ref})} \varphi - T \varphi \left( \frac{\partial}{\partial T} \right)_{\rho, \varphi} \mu_-^{(\text{ref})}. \quad (\text{F1})$$

The value of the last partial derivative above equals that of  $f_{\varphi T}$  in the middle of the reservoir in the reference state owing to  $f_{\rho\varphi} = 0$ . Thus, because of Eq. (26), Eq. (F1) consists of  $\bar{H}_-^{(\text{ref})} \varphi$  and the other term. This term gives an extra term

$$\frac{T_* \tau_*}{\mu_*} (\varphi f_{\varphi\varphi} \alpha_P)^{(\text{ref})} \hat{\psi}^{(0)} \quad (\text{F2})$$

to Eq. (48), where the superscript (ref) implies that the product in the parentheses should be evaluated in the middle of the reservoir in the reference state. We can use Eq. (52) to evaluate  $f_{\varphi\varphi}$  and find Eq. (F2) to be smaller than  $30|\tau|^\nu |\hat{\psi}^{(0)}|$  in magnitude. This magnitude is found to be much smaller than the corresponding magnitude given by the circles in

Fig. 3, with the aid of the results in Fig. 2. Thus, Eq. (F2) is negligible in deriving Eq. (45).

#### APPENDIX G: THERMOOSMOTIC FLOW FAR FROM A FLAT SURFACE

For a mixture occupying a semi-infinite space bounded by a flat wall surface, we consider imposing a temperature gradient along the  $z$  axis, which is parallel to the wall surface. The equilibrium profile  $\psi^{(0)}$  becomes a function of the distance from the surface, denoted by  $X$ , and is assumed to approach zero as  $X \rightarrow \infty$ . The velocity field in this situation can be obtained in the same way as Eq. (49) is derived. Assuming that  $\eta_s$  to be  $\eta_*$  homogeneously and using Eq. (58), we find that the  $z$  component of the mixture velocity far from the surface, or the slip velocity, is approximately given by

$$\frac{k_B C_1 |\tau|}{2\eta_* \xi_0^2 \tau} \int_0^\infty dX_1 \int_{X_1}^\infty dX \omega^{\nu-1} [\psi^{(0)}(X)]^2 \quad (\text{G1})$$

multiplied by the  $z$  component of the temperature gradient.

When the second term is much smaller than the first term on the r.h.s. of Eq. (41),  $\hat{\omega} \approx |\hat{\tau}|$  holds and the second term on the r.h.s. of Eq. (39) is negligible. We further approximate  $M_-$  to be  $k_B T_c C_1$  to obtain the free-energy density in the Gaussian model, where  $\xi$  becomes homogeneous and  $\psi^{(0)}(X)$  equals  $h\xi e^{-X/\xi}/M_-$  [97,98]. Substituting this into Eq. (G1) with  $\omega = |\tau|$  and  $h = 0.1 \text{ cm}^3/\text{s}^2$ , we find that the slip velocity in terms of  $\hat{v}_z^{(\text{th})}$  for a mixture of LW (NEMP) is  $-0.082$  (0.12) at  $|\tau| = 3.2 \times 10^{-3}$ , and  $-0.017$  (0.025) at  $|\tau| = 6.4 \times 10^{-3}$ . Here, for the critical exponents, we use the values mentioned in Sec. III C, not the values in the Gaussian model. These values of the slip velocity are comparable to the corresponding values calculated with the procedure used for Fig. 5, which are  $-0.042$  (0.061) at  $|\tau| = 3.2 \times 10^{-3}$  and  $-0.014$  (0.021) at  $|\tau| = 6.4 \times 10^{-3}$ .

The equilibrium profile  $\psi^{(0)}(X)$  becomes universal in the adsorption layer as the critical point is approached beyond the regime of the Gaussian model [32,41,42]. As is done for the diffusio-osmosis in Appendix D of Ref. [27] and in Sec. V C of Ref. [44], we use the universal profile  $\psi^{(0)}(X) \propto X^{-\beta/\nu}$  in Eq. (G1). With the aid of Eq. (41), we find that the resultant slip velocity in thermo-osmosis becomes proportional to  $|\tau|^{\nu-1}$  as  $\tau$  approaches zero.

- 
- [1] A. P. Bregulla, A. Würger, K. Günther, M. Mertig, and F. Cichos, Thermo-osmotic flow in thin films, *Phys. Rev. Lett.* **116**, 188303 (2016).
- [2] C. Lee, C. Cottin-Bizonne, A.-L. Biance, P. Joseph, L. Bocquet, and C. Ybert, Osmotic flow through fully permeable nanochannels, *Phys. Rev. Lett.* **112**, 244501 (2014).
- [3] S. Shin, Diffusiophoretic separation of colloids in microfluidic flows, *Phys. Fluids* **32**, 101302 (2020).
- [4] X. Wang, M. Liu, D. Jing, A. Mohamad, and O. Prezhd, Net unidirectional fluid transport in locally heated nanochannel by thermo-osmosis, *Nano Lett.* **20**, 8965 (2020).
- [5] S. Shakib, B. Rogez, S. Khadir, J. Polleux, A. Würger, and G. Baffou, Microscale thermophoresis in liquids induced by plasmonic heating and characterized by phase and fluorescence microscope, *J. Phys. Chem. C* **125**, 21533 (2021).
- [6] W. Q. Chen, M. Sedighi, and A. P. Jivkov, Thermo-osmosis in hydrophilic nanochannels: Mechanism and size effect, *Nanoscale* **13**, 1696 (2021).
- [7] R. Ganti, Y. Liu, and D. Frenkel, Molecular simulation of thermo-osmotic slip, *Phys. Rev. Lett.* **119**, 038002 (2017).
- [8] R. Piazza and A. Parola, Thermophoresis in colloidal suspensions, *J. Phys.: Condens. Matter* **20**, 153102 (2008).
- [9] A. Würger, Thermal non-equilibrium transport in colloids, *Rep. Prog. Phys.* **73**, 126601 (2010).
- [10] S. Marbach and L. Bocquet, Osmosis, from molecular insights to large-scale applications, *Chem. Soc. Rev.* **48**, 3102 (2019).



- [11] E. Mangaud and B. Rotenberg, Sampling mobility profiles of confined fluids with equilibrium molecular dynamics simulations, *J. Chem. Phys.* **153**, 044125 (2020).
- [12] S. Ramírez-Hinestrosa and D. Frenkel, Challenges in modelling diffusiophoretic transport, *Eur. Phys. J. B* **94**, 199 (2021).
- [13] B. V. Derjaguin, N. Churaev, and V. Muller, *Surface Forces* (Springer Science+Business Media, Berlin, 1987).
- [14] B. V. Derjaguin, Some results from 50 years' research on surface forces, in *Surface Forces and Surfactant Systems, Progress in Colloid & Polymer Science 74* (Steinkopff, Dresden, 1987), pp. 17–30.
- [15] J. L. Anderson, Colloid transport by interfacial forces, *Annu. Rev. Fluid Mech.* **21**, 61 (1989).
- [16] B. V. Derjaguin and G. P. Sidorenkov, On thermo-osmosis of liquid in porous glass, *Dokl. Acad. Nauk SSSR* **32**, 622 (1941).
- [17] B. V. Derjaguin, G. P. Sidorenkov, E. A. Zubashchenkov, and E. V. Kiseleva, Kinetic phenomena in boundary films of liquids, *Kolloidn. Zh.* **9**, 335 (1947).
- [18] B. V. Derjaguin, S. S. Dukhin, and M. M. Koptelova, Capillary osmosis through porous partitions and properties of boundary layers of solutions, *J. Colloid Interface Sci.* **38**, 584 (1972).
- [19] E. Y. Kenig, Y. Su, A. Lautenschleger, P. Chasanis, and M. Grünewald, Micro-separation of fluid systems: A state-of-the-art review, *Sep. Purif. Technol.* **120**, 245 (2013).
- [20] X. Hou, Y. Hu, A. Grinthal, M. Khans, and J. Aizenberg, Liquid-based gating mechanism with tunable multiphase selectivity and antifouling behaviour, *Nature (London)* **519**, 70 (2015).
- [21] G. Lippmann, Endosmose entre deux liquides de même composition chimique et de températures différentes, *Compt. Rend.* **145**, 104 (1907).
- [22] M. Aubert, Thermo-osmose, *Ann. Chim. Phys.* **26**, 145 (1912).
- [23] L. Fu, S. Merabia, and L. Joly, What controls thermo-osmosis? Molecular simulations show the critical role of interfacial hydrodynamics, *Phys. Rev. Lett.* **119**, 214501 (2017).
- [24] P. Anzini, G. M. Colombo, Z. Filiberti, and A. Parola, Thermal forces from a microscopic perspective, *Phys. Rev. Lett.* **123**, 028002 (2019).
- [25] R. Ganti, Y. Liu, and D. Frenkel, Hamiltonian transformation to compute thermo-osmotic forces, *Phys. Rev. Lett.* **121**, 068002 (2018).
- [26] K. Proesmans and D. Frenkel, Comparing theory and simulation for thermo-osmosis, *J. Chem. Phys.* **151**, 124109 (2019).
- [27] S. Yabunaka and Y. Fujitani, Isothermal transport of a near-critical binary fluid mixture through a capillary tube with the preferential adsorption, *Phys. Fluids* **34**, 052012 (2022).
- [28] D. Beysens and S. Leibler, Observation of an anomalous adsorption in a critical binary mixture, *J. Physique Lett.* **43**, 133 (1982).
- [29] M. Schlossman, X-L. Wu, and C. Franck, Order-parameter profile at long distances in an adsorbed binary liquid mixture near criticality, *Phys. Rev. B* **31**, 1478 (1985).
- [30] K. Binder, *Critical Behavior at Surfaces*, in Phase Transitions and Critical Phenomena, edited by C. Domb and J. L. Lebowitz (Academic Press, New York, London, 1983), Vol. 8, pp. 1–444.
- [31] H. W. Diehl, *Field-theoretic Approach to Critical Behavior at Surfaces*, in Phase Transitions and Critical Phenomena, edited by C. Domb and J. L. Lebowitz (Academic Press, New York, London, 1986), Vol. 10, pp. 76–267.
- [32] H. W. Diehl, The theory of boundary critical phenomena, *Int. J. Mod. Phys. B* **11**, 3503 (1997).
- [33] B. M. Law, Wetting, adsorption, and surface critical phenomena, *Prog. Surf. Sci.* **66**, 159 (2001).
- [34] L. Bocquet and E. Charlaix, Nanofluidics, from bulk to interfaces, *Chem. Soc. Rev.* **39**, 1073 (2010).
- [35] S. Yabunaka and Y. Fujitani, Drag coefficient of a rigid spherical particle in a near-critical binary fluid mixture, beyond the regime of the Gaussian model, *J. Fluid Mech.* **886**, A2 (2020).
- [36] K. Kawasaki, Kinetic equations and time correlation functions of critical fluctuations, *Ann. Phys. (NY)* **61**, 1 (1970).
- [37] J. V. Sengers, Transport properties near critical points, *Int. J. Thermophys.* **6**, 203 (1985).
- [38] E. D. Siggia, P. C. Hohenberg, and B. I. Halperin, Renormalization-group treatment of the critical dynamics of the binary-fluid and gas-liquid transitions, *Phys. Rev. B* **13**, 2110 (1976).
- [39] A. Onuki, *Phase Transition Dynamics* (Cambridge University Press, Cambridge, 2002), Secs. 2.3, 3.1, 4.3, and 6.5.
- [40] R. Folk and G. Moser, Critical dynamics: A field-theoretical approach, *J. Phys. A: Math. Gen.* **39**, R207 (2006).
- [41] M. E. Fisher and P. G. de Gennes, Phénomènes aux parois dans un mélange binaire critique, *C. R. Acad. Sci. Paris B* **287**, 207 (1978).
- [42] J. Rudnick and D. Jasnow, Order-parameter profile in semi-infinite systems at criticality, *Phys. Rev. Lett.* **48**, 1059 (1982).
- [43] Y. Fujitani, Diffusiophoresis in a near-critical binary fluid mixture, *Phys. Fluids* **34**, 041701 (2022).
- [44] Y. Fujitani, Effects of the preferential adsorption in a near-critical binary fluid mixture on dynamics of a droplet, *Phys. Fluids* **34**, 092007 (2022).
- [45] A. Onuki, Dynamic van der Waals theory, *Phys. Rev. E* **75**, 036304 (2007).
- [46] G. Gonnella, A. Lamura, and A. Piscitelli, Dynamics of binary fluid mixtures in inhomogeneous temperatures, *J. Phys. A: Math. Theor.* **41**, 105001 (2008).
- [47] R. Okamoto and A. Onuki, Casimir amplitude and capillary condensation of near-critical binary fluids between parallel plates: Renormalized local functional theory, *J. Chem. Phys.* **136**, 114704 (2012).
- [48] S. R. de Groot and G. Mazur, *Non-equilibrium Thermodynamics* (Dover, New York, 1984), Chaps. II, XI, and XV.
- [49] S. Kjelstrup, D. Bedeaux, E. Johannessen, and J. Gross, *Non-Equilibrium Thermodynamics for Engineers* (World Scientific, Singapore, 2017).
- [50] B. I. Halperin, P. C. Hohenberg, and E. D. Siggia, Renormalization-group calculations of divergent transport coefficients at critical point, *Phys. Rev. Lett.* **32**, 1289 (1974).
- [51] T. Ohta, Selfconsistent calculation of dynamic critical exponents for classical liquid, *Prog. Theor. Phys.* **54**, 1566 (1975).
- [52] R. F. Berg and M. R. Moldover, Critical exponent for the viscosity of four binary liquids, *J. Chem. Phys.* **89**, 3694 (1988).
- [53] R. F. Berg and M. R. Moldover, Critical exponent for viscosity, *Phys. Rev. A* **42**, 7183 (1990).
- [54] S. Z. Mirzaev, R. Behrends, T. Heimburg, J. Haller, and U. Kaatz, Critical behavior of 2, 6-dimethylpyridine-water: Measurements of specific heat, dynamic light scattering, and shear viscosity, *J. Chem. Phys.* **124**, 144517 (2006).
- [55] L. Mistutra, Transport coefficients near a critical point in multi-component fluid system, *Nuovo Cim. B* **12**, 35 (1972).

- [56] J. S. Walker and C. A. Vause, Reappearing phases, *Sci. Am.* **256**, 98 (1987).
- [57] M. Toda, S. Kajimoto, S. Toyouchi, T. Kawakatsu, Y. Akama, M. Kotani, and H. Fukumura, Phase behavior of a binary fluid mixture of quadrupolar molecules, *Phys. Rev. E* **94**, 052601 (2016).
- [58] Z. Chernia and Y. Tsori, Hydrogen bonding of dimethylpyridine clusters in water: Correlation between the lower consolute solution temperature and electron interaction energy, *J. Chem. Phys.* **152**, 204304 (2020).
- [59] A. Pelissetto and E. Vicari, Critical phenomena and renormalization-group theory, *Phys. Rep.* **368**, 549 (2002).
- [60] B. I. Halperin, P. C. Hohenberg, and S. Ma, Renormalization-group methods for critical dynamics: I. Recursion relations and effects of energy conservation, *Phys. Rev. B* **10**, 139 (1974).
- [61] T. A. Edison, M. A. Anisimov, and J. V. Sengers, Critical scaling laws and an excess Gibbs energy model, *Fluid Phase Equilib.* **150–151**, 429 (1998).
- [62] A. van't Hof, M. Laura Japas, and C. J. Peters, Description of liquid-liquid equilibria including the critical region with the crossover-NRTL model, *Fluid Phase Equilib.* **192**, 27 (2001).
- [63] M. del Mar Olaya, P. Carbonell-Hermida, M. Trives, J. A. Labarta, and A. Marcilla, Liquid-liquid equilibrium data correlation using NRTL model for different types of binary systems: Upper critical solution temperature, lower critical solution temperature, and closed miscibility loops, *Ind. Eng. Chem. Res.* **59**, 8469 (2020).
- [64] Y. Fujitani, Preferential adsorption in a near-critical binary fluid mixture as analyzed in the framework of the non-random two-liquid model, *Fluid Phase Equilib.* **580**, 114050 (2024).
- [65] I. Iwanowski, K. Leluk, M. Rudowski, and U. Kaatzte, Critical dynamics of the binary system nitroethane/3-methylpentane: Relaxation rate and scaling function, *J. Phys. Chem. A* **110**, 4313 (2006).
- [66] K. To, Coexistence curve exponent of a binary mixture with a high molecular weight polymer, *Phys. Rev. E* **63**, 026108 (2001).
- [67] A. M. Wims, D. McIntyre, and F. Hynne, Coexistence curve for 3-methylpentane-nitroethane near the critical point, *J. Chem. Phys.* **50**, 616 (1969).
- [68] J. K. Bhattacharjee, R. A. Ferrell, R. S. Basu, and J. V. Sengers, Crossover function for the critical viscosity of a classical fluid, *Phys. Rev. A* **24**, 1469 (1981).
- [69] B. C. Tsai and D. McIntyre, Shear viscosity of nitroethane-3-methylpentane in the critical region, *J. Chem. Phys.* **60**, 937 (1974).
- [70] A. Stein, S. J. Davidson, J. C. Allegra, and G. F. Allen, Tracer diffusion and shear viscosity for the system 2, 6-lutidine-water near the lower critical point, *J. Chem. Phys.* **56**, 6164 (1972).
- [71] C. A. Grattoni, R. A. Dawe, C. Y. Seah, and J. D. Gray, Lower critical solution coexistence curve and physical properties (density, viscosity, surface tension, and interfacial tension) of 2,6-lutidine+water, *J. Chem. Eng. Data* **38**, 516 (1993).
- [72] H. M. Leister, J. C. Allegra, and G. F. Allen, Tracer diffusion and shear viscosity in the liquid-liquid critical region, *J. Chem. Phys.* **51**, 3701 (1969).
- [73] M. M. Telo da Gama and R. Evans, The structure and surface tension of the liquid-vapour interface near the upper critical end point of a binary mixture of Lennard-Jones fluids I. The two phase region, *Mol. Phys.* **48**, 229 (1983).
- [74] D. Braun and A. Libchaber, Trapping of DNA by thermophoretic depletion and convection, *Phys. Rev. Lett.* **89**, 188103 (2002).
- [75] H.-R. Jiang, H. Wada, N. Yoshinaga, and M. Sano, Manipulation of colloids by a nonequilibrium depletion force in a temperature gradient, *Phys. Rev. Lett.* **102**, 208301 (2009).
- [76] Y. T. Maeda, A. Buguin, and A. Libchaber, Thermal separation: interplay between the Soret effect and entropic force gradient, *Phys. Rev. Lett.* **107**, 038301 (2011).
- [77] R. A. Omari, C. A. Grabowski, and A. Mukhopadhyay, Effect of surface curvature on critical adsorption, *Phys. Rev. Lett.* **103**, 225705 (2009).
- [78] D. Beysens, Brownian motion in strongly fluctuating liquid, *Thermodyn. Interfaces Fluid Mech.* **3**, 1 (2019).
- [79] F. J. Wegner, Corrections to scaling laws, *Phys. Rev. B* **5**, 4529 (1972).
- [80] Z. Y. Chen, P. C. Albright, and J. V. Sengers, Crossover from singular critical to regular classical thermodynamic behavior of fluids, *Phys. Rev. A* **41**, 3161 (1990).
- [81] Z. Y. Chen, A. Abbaci, S. Tang, and J. V. Sengers, Global thermodynamic behavior of fluids in the critical region, *Phys. Rev. A* **42**, 4470 (1990).
- [82] R. Folk and G. Moser, Critical dynamics in mixtures, *Phys. Rev. E* **58**, 6246 (1998).
- [83] S. Samin and R. van Roij, Interplay between adsorption and hydrodynamics in nanochannels: Towards tunable membranes, *Phys. Rev. Lett.* **118**, 014502 (2017).
- [84] P. G. De Gennes and J. Prost, *The Physics of Liquid Crystals* (Oxford University Press, Oxford, 1993).
- [85] Y. Fujitani, Dynamics of the lipid-bilayer membrane taking a vesicle shape, *Physica A* **203**, 214 (1994); [Erratum: Dynamics of the lipid-bilayer membrane taking a vesicle shape, **237**, 346 (1997)].
- [86] Y. Fujitani, Effective viscosity of a near-critical binary fluid mixture with colloidal particles dispersed dilutely under weak shear, *J. Phys. Soc. Jpn.* **83**, 084401 (2014).
- [87] J. Luettmer-Strathmann, Thermal diffusion in the critical region, in *Thermal nonequilibrium Phenomena in Fluid Mixtures, Lecture Notes in Physics* (Springer, Berlin, 2002), Vol. 584, pp. 24–37.
- [88] L. D. Landau and E. M. Lifshitz, *Fluid Mechanics*, 2nd ed. (Elsevier, Amsterdam, 1987), Sec. 58.
- [89] M. A. Anisimov, A. V. Voronel, and E. E. Gorodetskii, Isomorphism of critical phenomena, *Sov. Phys. JETP* **33**, 605 (1971).
- [90] M. Giglio and A. Vendramini, Thermal-diffusion measurements near a consolute critical point, *Phys. Rev. Lett.* **34**, 561 (1975).
- [91] I. I. Ryzhkov and S. V. Kozlova, Stationary and transient Soret separation in a binary mixture with a consolute critical point, *Eur. Phys. J. E* **39**, 130 (2016).
- [92] W. Köhler and K. I. Mozorov, The Soret effect in liquid mixtures—A review, *J. Non-Equilib. Thermodyn.* **41**, 151 (2016).
- [93] M. A. Anisimov, A. V. Voronel, and T. M. Ovodova, The behavior of thermodynamical quantities near the critical line

- of an incompressible liquid mixture, *Sov. Phys. JETP* **35**, 536 (1972).
- [94] M. A. Anisimov, E. E. Gorodetskii, V. D. Kulikov, A. A. Povodyrev, and J. V. Sengers, A general isomorphism approach to thermodynamic and transport properties of binary fluid mixtures near critical points, *Physica A* **220**, 277 (1995).
- [95] E. A. Clerke and J. V. Sengers, Fast pressure quenches near the critical point of a binary liquid mixture, *Physica A* **118**, 360 (1983).
- [96] F. Pousaneh, O. Edholm, and A. Maciołek, Molecular dynamics simulation of a binary mixture near the lower critical point, *J. Chem. Phys.* **145**, 014501 (2016).
- [97] Y. Fujitani, Undulation amplitude of a fluid membrane in a near-critical binary fluid mixture calculated beyond the Gaussian model supposing weak preferential attraction, *J. Phys. Soc. Jpn.* **86**, 044602 (2017).
- [98] Y. Fujitani, Relaxation rate of the shape fluctuation of a fluid membrane immersed in a near-critical binary fluid mixture, *Eur. Phys. J. E* **39**, 31 (2016).